Marine Pollution Bulletin
September 2022, Volume 182 Pages 113977 (13p.)
https://doi.org/10.1016/j.marpolbul.2022.113977
https://archimer.ifremer.fr/doc/00788/89950/

Ultraphytoplankton community structure in subsurface waters along a North-South Mediterranean transect

Boudriga Ismail [1?*], Thyssen Melilotus [2], Zouari Amel [1], Garcia Nicole [2], Tedetti Marc [2], Bel Hassen Malika [1]

[1] Institut National des Sciences et Technologies de la Mer (INSTM), 28 rue 2 mars 1934, Salammbô 2025, Tunisia
[2] Aix Marseille Uni., Université de Toulon, CNRS, IRD, MIO UM 110, 13288 Marseille, France

* Corresponding author : Ismail Boudriga, email address : mohamedismail.boudriga@instm.rnrt.tn

Abstract :

Here we assessed the subsurface ultraphytoplanktonic (< 10 µm) community along a North-South round-trip Mediterranean transect as part of a MERITE-HIPPOCAMPE cruise campaign in April–May 2019. Temperature, salinity, and nutrient concentrations in subsurface waters (2–5 m depth) were also measured along the transect. The subsurface ultraphytoplankton community structure was resolved with a spatial resolution of few kilometers and temporal resolution of 30-min intervals using automated pulse shape recording flow cytometry. The subsurface waters were clustered into seven areas based on temperature and salinity characteristics. Synechococcus were by far the most abundant group in all prospected zones, and nanoeukaryotes were the main biomass component, representing up to 51 % of ultraphytoplanktonic carbon biomass. Apparent net primary productivity (NPP) followed a decreasing gradient along the transect from north to south and was mostly sustained by Synechococcus in all zones. These findings are likely to have implications in terms of the trophic transfer of contaminants in planktonic food webs, as they highlight the potential role of nanoplankton in contaminants bioaccumulation processes and the potential role of Synechococcus in a likely transfer via grazing activities.

Keywords : Ultraphytoplankton community structure, Contaminants transfer, Nanoplankton, Synechococcus, High resolution cytometry, Growth rate, Net primary productivity

1. Introduction

Phytoplankton represents only 0.2% of global autotrophic biomass yet is responsible for roughly 50% of net primary production on Earth (i.e. 50 Pg C $year^{-1}$) (Falkowski et al., 1998; Field et al., 1998; Chavez et al., 2011). To understand the exact role of phytoplankton in biogeochemical cycles, the biological carbon pump (Siegenthaler and Sarmiento, 1993) and transfers of energy and matter within the trophic web (Sakka-Hlailli et al., 2014), it is essential to characterize the phytoplankton size spectrum, its communities and species and their relative production at the appropriate spatiotemporal scales.

Dynamic maps of phytoplankton distribution are affected by the sampling and measurement methods used. To illustrate, the size-fractional contribution of phytoplankton populations to bulk biomass can be measured by remote sensing using signatures of diagnostic pigments (Ciotti and Bricaud, 2006; Brewin et al., 2010; Hirata et al., 2011), but these large-scale observations suffer from low spatio-temporal scale resolution (Levy et al.,2003). Single-cell analyses using flow cytometry combined with *in situ* and automated sampling can observe fine-scale temporal dynamics of phytoplankton (Dubelaar and Gerritzen, 2000; Thyssen et al., 2008, 2014). The most efficient method for quantifying phytoplankton productivity is to estimate the phytoplankton division rate of a cell population. A good growth rate estimation can be achieved using several optical properties based on periodic increase and decrease in light scattering intensity, interpreted as a cell size-linked response in cellular growth and division during the cell cycle (DuRand, 2001; Binder et al., 1996). Diel variation in phytoplankton cell dimensions was used as an automated measurement to calculate growth rates of natural phytoplanktonic groups in surveys based on high-frequency flow cytometry (Sosik et al., 2003). This approach has been used to investigate the variability of primary production in different trophic

conditions, from eutrophic bloom areas (Campbell et al., 2010; Brosnahan et al., 2015) to oligotrophic ecosystems (Hunter-Cervera et al., 2014; Ribalet et al., 2015).

In the Mediterranean Sea, pigment analysis revealed that more than 80% of the autotrophic biomass originated from the nano- and pico-sized planktonic groups (Vidussi et al., 2001; Bel Hassen et al., 2009). These size fractions appear to play a crucial role in the energy transfer to higher trophic levels in mainly oligotrophic marine areas such as the Mediterranean Sea (Pulido-Villena et al., 2014). Moreover, the lower trophic levels of pelagic ecosystems, such as phytoplankton and heterotrophic prokaryotes, are particularly exposed to various metallic and organic contaminants for which bioconcentrations are governed by sorption between the surrounding water and the cells (Wallberg et al., 1997; Sobek and Gustafsson, 2004; Nizzetto et al., 2012). Characterizing these populations in terms of functional diversity, contribution to bulk fluorescence, carbon biomass and growth rate can therefore provide valuable information on their role not just in energy transfers but also in the potential accumulation and transfer of contaminants within planktonic food webs, which are strongly influenced by the species/size structure and biomass of the plankton community (Alekseenko et al., 2018; Chouvelon et al., 2019).

Here we investigated the subsurface ultraphytoplankton distribution along a North-South transect in the Mediterranean Sea using high-frequency pulse shape recording flow cytometry as part of the MERITE-HIPPOCAMPE cruise. This cruise set out to study the accumulation and transfer of metallic and organic contaminants at the atmosphere–water–plankton interfaces and within the planktonic food webs (phytoplankton, zooplankton and bacterioplankton) in areas of scientific and economic interest of the Mediterranean Sea. The main objectives of the research reported here were: 1) to characterize the ultraphytoplankton community structure in terms of abundance, biomass, red fluorescence, and apparent growth rate along the North-South Mediterranean transect that crosses areas featuring different physical structures, hydrological and biogeochemical conditions, and anthropogenic pressures, and 2) to assess the productivity of each resolved group in order to provide

clues on carbon turnover in the phytoplanktonic populations and their potential roles in the carbon cycle and consequently in contaminant transfers within the planktonic food webs.

2. Material and methods

2.1. Stations and sampling

The MERITE-HIPPOCAMPE cruise was carried out in spring, from 13 April and 14 May 2019, aboard the French Research Vessel (R/V) *Antéa*, along a North-South round trip transect from the French coast (La Seyne-sur-Mer; North-western Mediterranean Sea) to the Gulf of Gabès in Tunisia (South-eastern Mediterranean Sea) (Tedetti and Tronczynski, 2019) (Fig. 1). The investigation period was divided into two sub-periods, Leg 1 and Leg 2. Leg1, from 13 to 28 April, ran the southward transect between La Seyne-sur-Mer and Tunis, with sampling of five stations: St2, St4, St3, St10 and St11. Leg 2, from 30 April to 14 May, covered the southward end of the transect (from Tunis to the Gulf of Gabès) and then the return trip back northward, from the Gulf of Gabès to La Seyne-sur-Mer. Five stations were sampled during leg 2: St1, St9, St15, St17, and St19 (Fig. 1). These stations were chosen according to different criteria based on physical, biogeochemical and biological conditions and anthropogenic influences (see Tedetti et al., submitted). Table 1 summarizes the main characteristics and the strategy of selection of sampled stations. An extra station named 'Zarzis', where biological parameters were sampled but no nutrients were measured, has been added to sampling list.

Subsurface temperature and salinity were recorded continuously at high frequency all along the transect from flow-through pumped seawater at 2-m depth, using a thermosalinograph (TSG, SeaBird SBE 21). A chamber for subsampling the flow-through seawater was plugged for automated flow cytometry measurements. At the ten stations, *in situ* measurements were performed along with several further operations to collect water, particles and plankton (see details in Tedetti et al., submitted), including the deployment of a trace metal-clean carousel equipped with ten 12-L bottles (1 Niskin, 5 Niskin-X, 4 Go-Flo) and a conductivity-temperature-depth probe (CTD; Seabird SBE 911*plus*). This system was used to capture vertical profiles of temperature, salinity, and total chlorophyll *a* (TChl*a*)

in the water column, in subsurface seawater (5-m depth) and at the deep chlorophyll maximum (DCM) for analysis of various parameters including nutrients, TChl*a*, pigments, dissolved and particulate organic carbon, and metallic trace elements.

2.2. Nutrients

Seawater for nutrient analyses was collected at 5-m depth and in the DCM using Niskin-X bottles (i.e. Niskin with a free Teflon-coated sample chamber; model 101012X). On-board in-line filtration was performed from the Niskin-X bottles using an argon pressure system. The bottles were pressurized to 0.5 bar with argon (UN1006, compressed, 2.2) with their stoppers held tight by home-made high-density polyethylene (HDPE) clamps. A 10-cm-long piece of acid-cleaned silicon tubing was inserted into the drainage tap of each bottle, and perfluoroalkoxy (PFA) resin filter holders (Savillex®) were connected to the tubing. Pre-combusted (450°C, 6 h) glass fiber filters (GF/F, 25-mm diameter, Whatman) were fitted in the filter holders. After rinsing the filters with several hundred mL of seawater, filtered (~0.7 µm) samples were collected into cleaned 50-mL polycarbonate bottles and immediately frozen and stored on board at -18°C for laboratory nutrient analyses A few days after the cruise campaign. Nitrate (NO_3^-), nitrite (NO_2^-) and phosphate (PO_4^{3-}) ions were analyzed by standard automated colorimetry procedure using a Seal Analytical continuous-flow AutoAnalyser III (AA3) as per the protocol described by Aminot and Kérouel (2004, 2007) (detection limits of 0.05 µM for NO_3^- and 0.02 µM for NO_2^- and PO_4^{3-}). Ammonium (NH_4^+) ions were analyzed by fluorescence as per Holmes et al. (1999) and Taylor et al. (2007).

2.3. Automated flow cytometry

We used the CytoSense automated flow cytometer (CytoBuoy b.v. (NL)) designed to study individual or colonial phytoplankton cells between 0.8 and 800 µm to analyzed seawater from the continuous flow-through system pumped at 2-m depth, at a rate of 1 L min^{-1}, filling an intermediate

300-mL container isolating the subsample to minimize the spatial extent during the analytical window. A weighted calibrated peristaltic pump set at 5 µL $s^{-1}$was used to sample the seawater. The sample was then surrounded by a sheath loop (0.2-µm-filtered NaCl solution 35‰) to separate, align, and drive the particles to the light source (OBIS Coherent laser, 488 nm, 120 mW), and continuously recycled using a set of two 0.1-µm filters. The light scattered in front of the laser beam (forward scatter, FWS) was collected on two left and right photodiodes and used for laser alignment control. The light scattered orthogonally (sideward scatter, SWS) and fluorescence emissions were separated by a set of optical filters (SWS, 488 nm), yellow fluorescence (FLY, 506–601 nm), orange fluorescence (FLO, 601–650 nm) and red fluorescence (FLR, > 650 nm), and collected on photomultiplier tubes. Fluorescent beads measuring 3 µm (Cyto-Cal™) and 10 µm (Polybead®) in diameter were used every 24–72 h to normalize fluorescence and size. Silica beads (Bangs lab®, silica microspheres) measuring 1.0, 2.02 and 3.13 µm were used for size estimation of phytoplankton cells.

Ultraphytoplankton groups were optically resolved based on their light-scattering and fluorescence properties. Two successive samples triggered on two FLR signals linked to chlorophyll emission (with values of 10 and 20 mV) were acquired according to frequency of the events. The phytoplankton groups were classified using Cytoclus© software. Each cell was thus characterized by a set of optical pulse shapes that constitute the cytometric signature. Microsphere beads (3 µm, Polyscience®) were used to discriminate between picophytoplankton and nanophytoplankton.

Cell biovolume was estimated from a calibration curve plotted between different pre- size microbeads and their equivalent cytometric FWS signature. The following relationships were established for picophytoplankton (Eq. 1) and nanophytoplankton (Eq. 2):

$$\text{Log(Biovolume)} = 0.2132 \times \text{Log(FWS)} - 1.161 \quad \text{(Eq. 1)}$$

$$\text{Log(Biovolume)} = 1.1104 \times \text{Log(FWS)} - 10.426 \quad \text{(Eq. 2)}$$

Eq. 2 was modified and adapted from Foladori et al. (2008) and Dugenne et al. (2016). A carbon biomass conversion factor was assigned to each population as follows: *Synechococcus* abundances

were converted using the estimation of 200 fg C $cell^{-1}$ (Mackey et al., 2002), and picoeukaryote and nanoeukaryote carbon biomass were calculated using the equation of Verity et al. (1992):

$$Qc,cal = a\ V^{0.866} \quad \text{(Eq. 3)}$$

where Qc,cal is estimated average carbon biomass per cell (in fg C $cell^{-1}$), V is biovolume (μm^3) and "a" is values of 0.39, 0.32, 0.27 and 0.25 for *Synechococcus*, picoeukaryotes, nanoeukaryotes and cryptophyte-like organisms, respectively. Table 2 reports the Qc,cal for each group.

Daily growth rate was estimated using the ratio between minimum and maximum mean cell biovolume (Eq. 4) (Binder et al., 1996; Vaulot and Marie, 1999). This approach assumes that the population synchronizes between the growth and division phases:

$$\mu\_ratio=Log(V\_max/V\_min) \quad \text{(Eq. 4)}$$

where μ_{ratio} is daily growth rate (d^{-1}), and V_{max} and V_{min} are minimum and maximum mean cell biovolumes (μm^3 $cell^{-1}$). The apparent increase in carbon biomass, defined as net primary production (NPP in mg C m^{-3} d^{-1}) (Eq. 5), was calculated using the carbon conversion factor Qc,cal (Table 2) as a scalar product with N (abundance) and exponential growth rate:

$$NPP=Q\_(c,cal)\times[e\^(\mu\_ratio\ )-1]\times N \quad \text{(Eq. 5)}$$

2.4. Data analysis

Hierarchical clustering was used to discriminate between the different surface water properties based on their surface temperature and salinity values. A distance matrix describing the dissimilarities of these parameters was constructed. The data were grouped using complete-linkage clustering according to Euclidean (root mean squared) distances. The TS plot illustrating the different water-sample properties was then elaborated using the ODV 5.4.0 software developed by R. Schlitzer at the AWI. Surface-water velocity for the sampled days was computed from the Copernicus climate change service infrastructure website (https://marine.copernicus.eu/).

3. Results

3.1. Hydrological features

Subsurface temperature distribution showed relative homogeneity during the two investigated legs (Fig. 2B), with the coldest waters recorded in the northern stations and warmer waters recorded towards the southern stations. Subsurface salinity distribution also showed homogeneity between the two legs (Fig. 2A), with values decreasing from north to south except for a slight increase in the coastal area of the Gulf of Gabès.

The lowest temperatures (~14.0°C) were observed in the Bay of Marseille, while the highest temperatures were measured in the southern Tunisia coastal waters, with a maximum of 19.5°C recorded near Djerba and Zarzis (Fig. 2B). The highest salinity values were found in the Ligurian region, with a maximum of 38.50. The lowest salinity values (i.e. 37.12) were found in the northern Tunisian coastal waters, particularly in the Gulf of Tunis and in the Sicily Strait (Fig. 2A).

Hierarchical clustering carried out on these subsurface temperature and salinity values distinguished 7 geographic zones (Z1 to Z7) colour-mapped in Figure 3A and 3B. Each zone encompasses a different number of stations: Z1 encompasses stations 1, 2, 3 and 4, Z2 encompasses station 9, Z3 encompasses stations 10 and 11, Z4 encompasses station 15, Z5 encompasses station 17, Z6 encompasses station 19, and Z7 encompasses the station called “Zarzis”. Subsurface temperature and salinity values varied from 13.8–15.5°C and 38.12–38.21 in the northern basin (i.e. Z1) to 15.8–17.4°C and 37.13–37.45 in the mid-track basin (i.e. Z4) and 19.2–19.9°C and 37.8–38.0 in the southern basin (i.e. Z7). For the other zones, temperature and salinity varied in the northern segment as follow :14.5–15.0°C and 38.2–38.4 in Z2, 14.9–16.9°C and 37.3–38.1 in Z3, and in the southern segment:16.8–17.8°C and 37.2–37.5 in Z5, 17.8–18.7°C and 37.5–37.7 in Z6.

The surface velocity map computed for the 8th of May 2019 (Fig. 4) and corresponding to the sampling date of station 9 shows an increased water velocity southwest of stations 9 and 10 likely corresponding to the edge of the seasonal northern Balearic front.

3.2. Nutrient concentrations

Nutrient concentrations measured at the 10 stations in subsurface waters (5-m depth) showed large differences between the different zones (Fig. 5): NH_4^+ varied from 0.007 to 0.790 µM, NO_3^- + NO_2^- varied from 0.05 to 0.63 µM, PO_4^{3-} varied from 0.03 to 0.34 µM, and $Si(OH)_4$ varied from 0.7 to 2.2 µM. Nutrient concentrations were relatively high at St4 and St9 (belonging to zones Z1 and Z2), particularly for NO_3^- + NO_2^- at St4 and $Si(OH)_4$ and PO_4^{3-} at St9. PO_4^{3-} concentration was also high in zone Z6. Redfield N/P ratio (Redfield et al., 1963) varied between 0.24 and 58 but in most stations, it was below 16, which points to a potential nitrogen limitation, except in St4 where it reached 58 which signals potential phosphorus limitation. Overall, nutrient concentrations following a decreasing gradient southward (Fig. 5), with the western basin being relatively mesotrophic and the eastern basin relatively oligotrophic.

3.3. Phytoplankton community distribution and composition

The functional groups were resolved based on the flow-cytometric optical signals from single cell biological features: FWS, SWS, FLR and FLY. Four groups of small plankton < 10 µm sized cells) were determined according to the optical properties of the cells (Fig. 6A, B). The plots of FLR *vs.* FLY and FLR *vs.* SWS differentiated two phycoerythrin-rich groups: one was differentiated by high FLY (phycoerythrin) emissions and a small computed estimated size of 1.05 ± 0.09 µm (Table 2), and was identified as *Synechococcus*, and the other showed a high FLY and a computed estimated size of 5.69 ± 0.77 µm and was identified as cryptophytes-like. Picoeukaryote and nanoeukaryote cells showed high FLR and low FLY emissions with a computed estimated size of 2.45 ± 0.19 µm and 4.16 ± 0.16 µm, respectively (Table 2).

Significant spatial heterogeneity in the distribution of ultraphytoplankton was observed throughout the sampling area (Fig. 7). Total ultraphytoplankton abundance was highest in the northern Ligurian basin (Z1 and Z2) and off the Zarzis coast (Z7) (Fig. 7A). FLR per unit of volume, used as a

proxy of TChl*a* content, was highest in zones Z1 and Z2 (Fig. 7B), with a maximum of 5.10^{12} a.u. m^{-3}, and moderately high off Zarzis (10^{12} a.u. m^{-3}). Total ultraphytoplankton carbon biomass (Fig. 7C) fluctuated between 50 and 125 mg C m^{-3} in certain coastal zones, such as south of Z7 and north of Z1, and up to 150 mg C m^{-3} in Z2.

Like total ultraphytoplankton abundance (Fig. 7A), the relative abundance of each group showed similar spatial patterns of distribution but with more contrasted gradients between zones (Fig. 8A). In general, abundances varied by a factor of up to 10 from the coast of Sardinia (Z4) and the Gulf of Gabès (Z5-Z6) to the northern Balearic front (Z2) and southern Tunisian coasts (Z7), as illustrated by *Synechococcus* abundances which varied from 3.4–9.8 10^9 cells m^{-3} to 30.8–86.9 10^9 cells m^{-3}. In terms of mean cell size (Fig. 8B), the zones from Z1 to Z3 in the north of the transect showed larger *Synechococcus* cells (> 1 µm) and smaller picoeukaryotes and cryptophyte-like cells (< 2.5 µm/cell and < 5.5 µm/cell, respectively). The mean size distribution of nanoeukaryotes did not vary significantly and was between 3.8 and 4.6 µm in most waters sampled.

FLR per cell followed roughly the same pattern of distribution than the abundances (Fig. 8C), and the highest FLR-per-cell values were mainly recorded in the areas that represented the highest abundances. FLR per cell within each group varied by a factor of up to 3 in Z2 for small size-fractions (*Synechococcus* and picoeukaryotes), 4 for cryptophytes-like fractions, and 5 for nanoeukaryotes.

Conversely, peaks in abundance correlated with minima in mean cell size. This pattern was particularly highlighted in Z2 (Fig. 8 and Fig. 10), especially for *Synechococcus* and picoeukaryotes with abundances ranging from 30.8 to 86.9 10^9 cells m^{-3} and 1.7 to 3.8 10^9 cells m^{-3} and mean cell size ranging from 0.9 to 1.4 µm and 2.1 to 2.6 µm, respectively.

Nanoeukaryotes and *Synechococcus* cells contributed the most to FLR per unit of volume in the 7 identified zones (Fig. 9B), with carbon biomasses (Fig. 9A) reaching up to 70 and 30 mg C m^{-3}, respectively (Table 3). Relative contributions of nanoeukaryotes and *Synechococcus* were highest in coastal areas, at up to 51% and 22%, respectively, in the Gulf of Gabès (Z7) but about 62.1% and

19.3%, respectively, in the Ligurian Basin (Z2) (Table 3). Cryptophyte-like cells were relatively low contributors to total biomass, and their carbon content varied considerably among zones, being up to 3 times higher in Z2 and Z7 than in the other areas (Table 3). The transition from coastal zone to offshore areas was characterized by a reversal in the pattern of contribution of *Synechococcus* and picoeukaryotes to carbon biomass, with *Synechococcus* contributing more in coastal areas whereas picoeukaryotes contributed more in areas farther offshore (Fig. 9A).

Analysis of the spatial distribution of median-normalized abundance, mean size and mean FLR_{cell} according to the identified physical characteristics of the water showed that three zones stand out from the others in terms of abundance, mean cell size and red FLR_{cell} (Fig. 10), namely zones Z1 and Z2 in the north of the Ligurian basin and zone Z7 on the edge of Zarzis. These areas are characterized by relatively high cell abundances of *Synechococcus* and cryptophytes-like cells compared to the other areas (Fig. 10A). In terms of mean cell size (Fig. 10B), these same areas showed relatively smaller cells with values below the median-normalized sizes for all groups, which probably reflects diurnal cell cycles that differ from one area to another. The estimated growth rates (Fig. 11) varied between the identified groups. Growth rates were lowest for nanoeukaryotes but highest were for cryptophyte-like cells and *Synechococcus*, with cryptophyte-like cells reaching more than two divisions per day in Z3, Z4 and Z6. This yielded a NPP of about 36.6 mg C m^{-3} d^{-1} in Z2 and 15.8 mg C m^{-3} d^{-1} in Z1 in the northern Mediterranean, mostly driven by *Synechococcus* and nanoeukaryotes, 5.8 mg C m^{-3} d^{-1} in Z4 in the central Mediterranean, and about 11 mg C m^{-3} d^{-1} in Z6 and Z7 in the southern Mediterranean (Table 4).

4. Discussion

The general pattern of circulation in the western basin of the Mediterranean Sea is characterized by Atlantic Water (AW) carried from the Algerian basin on to the Liguro-Provençal limit, thus forming the North Balearic front (Millot et al., 1991; Millot and Taupier-Letage, 2005). This hydrological

structure emerged here (Fig. 4) and corresponded to Z2 characterized by a high salinity over 38.5 and a low temperature of 14°C–15°C. Like all frontal zones, this area featured high nutrient concentrations, particularly in terms of nitrate, silicate, and phosphate (Estrada et al., 1996). The spatial distribution of ultraphytoplankton is known to be dependent on meso-scale or sub-mesoscale hydrodynamic features (Denis et al., 2010) like fronts that generate distinct water masses particularly in the Mediterranean Sea .

The part of the AW that progresses through the southern part of the Sardinian Channel continues along the embankment then crosses the Strait of Sicily to enter the eastern basin, where it ultimately feeds the Atlantic Tunisian Current (ATC). The ATC flows eastward mainly along the 200-m isobath (Beranger et al., 2005) and splits into two branches south of Lampedusa. The first branch flows directly toward the southern part of the Levantine basin, while the second branch flows over the Tunisian shelf and divides into two sub-branches: one invades the Tunisian shelf in the Gulf of Gabès and recirculates anticyclonically on the shelf, while the other continues flowing south-eastward as an important coastal current and reaches close to the Libyan coast (Jaber et al., 2014). The salinity barrier of 37.5 characterizing the AW in the Gulf of Gabès (Bel Hassen et al., 2009) was detected at the entrance of the Gulf corresponding to Z5 (Fig. 3A), but once it mixes with the high salinity of the coastal waters of the Gulf, the AW becomes harder to detect, as in zones Z6 and Z7.

Towards the south a decreasing nutrient gradient, mainly for nitrogen, and a gentle increase in phosphate at station St19 were observed. The meteorological conditions during this period were characterized by a dust storm accompanied with weak rainfall (< 1 mm). A high concentration of PO_4^{3-} , in zone Z6, i.e. 1.06 µM of PO_4^{3-} measured in the rainfall water collected on board, was potentially due to atmospheric inputs of nutrients from a Saharan dust episode that occurred on 03/05/2019. Atmospheric input from dust storms was previously confirmed as a main source of phosphorus in the coastal water (Guieu et al., 2014), and annual inputs in areas like the Gulf of Gabès were demonstrated to be the highest in the south Mediterranean (Markaki et al., 2010; Khammeri et al., 2018). Overall,

there was not an evident gradient in the abundance of the ultraphytoplankton fraction between the northern mesotrophic part and the southern oligotrophic part of the Mediterranean (Fig. 6). The maximum values for abundance, FLR_{cell} and biomass were all recorded in the Balearic frontal area (Z2), confirming that large-scale phytoplankton distribution in the Mediterranean was specifically affected by current hydrodynamics (Casotti et al., 2003; Denis et al., 2010). This area was particularly rich in silicate and phosphate and showed the highest abundance of larger size-fractions (nanoeukaryotes and cryptophyte-like cells) ($P < 0.05$ and $R^2 > 0.7$) (Fig. 7), confirming that low-nutrient regions are dominated by small phytoplankton, mostly *Synechococcus, Prochlorococcus* and picoeukaryotes, whereas more productive regions support not only these small cells but also abundant larger species (Raimbault et al., 1998; Hirata et al., 2011).

Synechococcus were by far the most abundant group in all prospected zones, although their highest relative biomass was reached in the Gulf of Gabès (Table 3). We did not manage to resolve *Prochlorococcus* in this study. The non-resolution of *Prochlorococcus* in subsurface water using a CytoSense could be related to their dim fluorescence signature due to the predominant high light intensity affecting surface waters in April-May combined with high background noise in the sheath fluid as no coal filter was used to lower the trigger level. The use of coal filter has been shown to greatly improve the resolution of this group (Marrec et al., 2018). Nevertheless, samples from the DCM were analyzed using the same instrument and showed the presence of *Prochlorococcus* at depths below 50 m (data not shown). This is consistent with previous patterns observed along the Tunisian coasts, with the presence of *Prochlorococcus* in warm stratified water at more than 60 m in depth (Khemmari et al., 2020; Quéméneur et al., 2020). Nonetheless, this dominance of *Synechococcus* over *Prochlorococcus* in the Mediterranean has already been reported and confirms the fact that *Synechococcus* is better adapted to the general hydrodynamic and nutrient conditions in the Mediterranean Sea (Denis et al., 2010).

Synechococcus had a mean estimated size and associated biovolume of 1.05 ± 0.09 µm and 0.6 ± 0.17 µm^3, respectively (Table 2), which fall within the range of 0.8 to 1.2 µm and 0.25 to 1.00 µm^3 reported in previous studies (Morel et al., 1993; Shalapyonok et al., 2001; Sosik et al., 2003; Hunter-Cevera et al., 2014; Marrec et al., 2018). Relatively smaller *Synechococcus* cells with values below the median of normalized sizes were observed in the lower-latitude warm southern Tunisian waters (Fig. 9B), confirming that their distribution appears to be principally controlled by water temperature and latitude (Pittera et al., 2014). This would also point to a likely genomic differentiation within this group, although a dominance of the clade III has been reported in the Mediterranean Sea, but without ruling out ecologically meaningful fine-scale diversity within the currently defined *Synechococcus* clades (Farrant et al., 2016).

Mean size of the main functional nanoeukaryote group observed was 4.15 ± 0.16 µm (Table 2), which is consistent with the value of 4.1 ± 0.5 µm reported by Marrec et al. (2018) in the north-western Mediterranean Sea. There were no significant variations in mean size of nanoeukaryotes observed along the transect (Fig. 9B), suggesting that this community might be dominated by similar genera. Indeed, the major feature of the Mediterranean basin in various regions and seasons is a biomass dominated by Prymnesiophytes (Latasa et al., 1992; Claustre et al., 1994; Bustillos-Guzman et al., 1995; Vidussi et al., 2000) with the genus Chrysochromulina (3.2–4.0 µm) largely represented in the north-western Mediterranean (Percopo et al., 2011). Conversely, the contribution of Prymnesiophytes to chlorophyll biomass, which is considered a prominent feature in the Mediterranean, was found to be relatively low in the Gulf of Gabès (Bel Hassen et al., 2008; 2009a), which was mainly explained by the dominance of smaller chlorophyll b-containing nanoplankton like prasinophytes. Nanoeukaryotes were the main contributors to total phytoplankton (> 60%) in terms of pigment content (defined by FLR) and carbon biomass. The contribution of nanoeukaryotes and picoeukaryotes in terms of pigment content fluctuated between 80% and 84% in the central Mediterranean, and between 69% and 77% in both the northern and southern Mediterranean (Table 3) where the prokaryotes

(*Synechococcus*) shown their highest contribution (15%–18.9% of FLR). This is less than the prokaryote contribution (32%–47%) to total Chl*a* reported by Barlow et al. (1997) using a chemotaxonomic approach in the southern Mediterranean region and less than the 26% in spring and 28% in summer found by Bel Hassen et al. (2009a) in the Gulf of Gabès. These deviations could be explained in part by the presumed contribution of *Prochlorococcus* in surface water that we were unable to resolve in this case. Indeed, when comparing the only contribution of *Synechococcus* in the Gulf of Gabès (15-17%) (Table 3) we found consistent values (15% in mean) with what reported using chemotaxonomic approach in the same area for the same period (Bel Hassen et al., 2009a).

Growth rates estimates computed from the difference in minimal and maximal values of biovolume showed that the highest rates were observed for the orange-fluorescing phycoerythrin-containing cells, i.e. cryptophyte-like cells and *Synechococcus*. Growth rate estimates for *Synechococcus* fluctuated between 0.38 and 1.1 d^{-1}, which is consistent with the values of 0.48–0.96 d^{-1} reported by Ferrier-Pages and Rassoulzadegan (1994) and 0.49 d^{-1} reported in the north-western Mediterranean Sea by Marrec et al. (2018). Growth rate estimates for cryptophyte-like cells were highly variable (0.3–1.7 d^{-1}) in Z1 but still consistent with the rate of 0.75 d^{-1} determined in spring 2004 in the center of the Liguro-Provençal basin (Gutierrez-Rodriguez et al., 2010). The computed apparent NPP rates of *Synechococcus* were the highest in Z1 (1.3–12 mg C m^{-3} d^{-1}) and Z2 (13.9–23 mg C m^{-3} d^{-1}). These NPP values were higher than the range of 0.01–1 mg C m^{-3} d^{-1} reported by Agawin et al. (1998) over the course of 1997–1998 (February to May) based on a biovolume-to-C conversion, and also higher than the value of 2.68 mg C m^{-3} d^{-1} reported by Marrec et al. (2018) in the north-western Mediterranean Sea during the autumn season. These studies used different approximations to calculate the biovolume-to-cellular carbon content. However, Marrec et al. (2018) demonstrated that cyanobacteria NPP rates obtained from different calculations provide similar specific C uptake rates, suggesting that these populations follow a daily dynamic at equilibrium. Nanoplankton was expected to be the main contributor to NPP due to its high abundance and high

cellular carbon content (Table 3), but its growth rate was relatively low, at generally under 0.3 d^{-1} which was even lower than the range (0.48–2.4 d^{-1}) previously reported in north-western Mediterranean (Ferrier-Pages and Rassoulzadegan, 1994), and could explain this low NPP, particularly in the central Mediterranean and off the northern Tunisian coast. Note that the NPP estimate does not integrate any of the cell removal processes driven by grazing or physical transport. Even if this estimation is valuable for all the resolved groups, the grazing pressure on nanoplankton and its motile capabilities nevertheless remain largely underestimated. Indeed, active top-down control of ultraphytoplankton has been widely suspected in the southern Tunisian coasts (Hamdi et al., 2015; Khammari et al., 2020) where it could prevent accumulations of nanoeukaryotes. Moreover, the approach used to calculate growth rate based on the ratio between maximum and minimum cell biovolume (Binder et al., 1996; Vaulot and Marie, 1999) assumes that cell growth and division are separated in time (synchronous population), whereas these processes occur simultaneously in a population. In general, growth-rate calculation based on cell size distribution enables a better estimation than Log(Vmax/Vmin) ratio, especially for asynchronized populations like nanoeukaryotes and cryptophyte-like cells. The NPP of picoeukaryotes ranged from 0.48 to 19 mg C m^{-3} d^{-1}, which is consistent with range of picoplankton production rates of 2.2–19.6 mg C m^{-3} d^{-1} compiled by Magazzu and Decembrini (1995) in the Mediterranean Sea.

Except in the Gulf of Gabès (Z6 and Z7), which is submitted to atmospheric forcing events, NPP followed a decreasing gradient along the North-South transect, confirming the general trend observed in the Mediterranean based on the all-size phytoplankton population (Colella et al., 2003). The size-fractioned NPP assessment conducted here focused on the size under < 10 µm, which has been demonstrated to represent 20% of NPP measured by ^{14}C particulate organic carbon production rates in a NW coastal Spanish station (Cermeno et al., 2006). Our decision to focus on this size fraction was prompted by their high contaminant accumulation capacities (see this issue). Determining the groups

that present the highest carbon assimilation capacity could provide key insight for characterizing the phytoplankton most involved in contaminant transfer in the trophic chain.

5. Conclusions

This campaign using high-frequency monitoring on subsurface ultraphytoplankton along a North-South Mediterranean round-trip transect led to the following conclusions:

- The Balearic frontal region showed the highest ultraphytoplankton abundances and biomasses, mostly attributed to *Synechococcus* and nanoplankton. Productivity was mostly sustained by *Synechococcus*. This pattern confirms the general statement that hydrodynamics is an important factor shaping the structure of this ultraphytoplanktonic community.
- *Synechococcus* was by far the most abundant group in subsurface water, with high biomass concentrations in the coastal zones reaching up to 22% in the Gulf of Gabès.
- Nanoplankton represented up to 51% of the total ultraphytoplankton biomass in all zones. If we consider that the transfer of contaminants to phytoplankton species is mainly biomass-related, then nanoplankton will be the relevant group to monitor. The straight conclusion leading out from this result is that the southern Tunisian coastal waters, which had the lowest nanoplanktonic biomasses, were probably the ecosystem that least accumulates contaminants in its trophic chain
- *Synechococcus* drove the highest carbon turnover in almost all zones surveyed. The contribution of *Synechococcus* to contaminant transfer up to higher trophic levels is largely dependent on the grazing potential.

Acknowledgements. The MERITE-HIPPOCAMPE cruise was organized and supported by the French Oceanographic Fleet (FOF), CNRS/INSU, IFREMER, IRD, the Tunisian Ministry of Agriculture, Water Resources and Fisheries and the Tunisian Ministry of Higher Education and

Scientific Research. It was funded by the cross-disciplinary "*Pollution & Contaminants*" axis of the CNRS-INSU MISTRALS program, as well as the IRD French-Tunisian International Joint Laboratory (LMI) 'COSYS-Med', the MIO Action Sud and Transverse Axis programs, the IRD Ocean Department, and the IFREMER. The MERITE-HIPPOCAMPE cruise is a joint action co-led by the MISTRALS program the MERITE-MERMEX and CHARMEX projects, the LMI COSYS-Med, and the MIO 'CONTAM' Transverse Axis. We thank the principal investigators (PIs) of the MERITE-HIPPOCAMPE project, J. Tronczynski (IFREMER), M. Tedetti, F. Carlotti, M. Pagano and C. Garnier (MIO), as well as the captain and crew of the R/V *Antéa* for their help and assistance during the cruise. We also thank C. Sammari and INSTM, the IRD's representation in Tunisia, and the French Institute of Tunisia for providing valuable logistics and financial assistance to help prepare the cruise. We thank the MIO's Service Atmosphère-Mer (SAM) platform and particularly D. Malengros for the preparation and management of the embarked material, the MIO's Plateforme Analytique de Chimie des Environnements Marins (PACEM platform) for performing the nutrient analyses, and K. Desboeufs (LISA) for providing nutrient concentrations in rainwater samples.

References

Alekseenko, E., Roux, B., Sukhinov, A., Kotarba, R., and Fougere, D., (2013). Coastal hydrodynamics in a windy lagoon. Comput. Fluids 77, 2435.

Aminot, A., Kérouel, R., (2004). Hydrologie des écosystèmes marins. Paramètres et analyses Ed. Ifremer, 336 p.

Aminot, A. and Kérouel, R., (2007). Dosage automatique des nutriments dans les eaux marines: Méthodes en flux continu, Edition Quae, Ifremer, Plouzané, France.

Ayata, S.D., Irisson, J.O., Aubert, A., Berline, L., Dutay, J.C., Mayot, N., Nieblas, A.E., D'Ortenzio, F., Palmieri, J., Reygondeau, G., Rossi, V., Guieu, C., (2018). Regionalisation of the Mediterranean basin, a MERMEX synthesis. Progress in Oceanography, 163, 7–20. doi: 10.1016/j.pocean.2017.09.016.

Bel Hassen, M., Drira, Z., Hamza, A., Ayadi, H., Akrout, F., Issaoui, H., (2008). Summer phytoplankton pigments and community composition related to water mass properties in the Gulf of Gabes. Estuarine, Coastal and Shelf Science 77,645–656.

Barlow, R.G., Mantoura, R.F.C., Cummings, D.G., Fileman, T.W., (1997). Pigment chemotaxonomic distributions of phytoplankton during summer in the western Mediterranean. Deep-Sea Research II 44, 833–850

Bel Hassen, M., Drira, Z., Hamza, A., Ayadi, H., Akrout, F., Messaoudi, S., Issaoui, H.,Aleya, L., Bouain, A., (2009a). Phytoplankton dynamics related to water mass properties in the Gulf of Gabes: Ecological implications. Journal of Marine Systems 75, 216–226.

Bel Hassen M., Hamza A., Drira Z., Zouari A., Akrout F., Messaoudi S., Aleya L., Ayadi H., (2009b). Phytoplankton-pigment signatures and their relationship to spring–summer stratification in the Gulf of Gabes. Estuarine, Coastal and Shelf Science, 83(3), 296–306, ISSN 0272-7714, https://doi.org/10.1016/j.ecss.2009.04.002.

Béranger, K., Mortier, L., Gasparini, G.P., Gervasio, L., Astraldi, M., Crepon, M., (2004). The dynamics of the Sicily Strait: a comprehensive study from observations and models. Deep-Sea Research II 51, 411–440.

Binder, B.J., Chisholm, S.W., Olson, R.J., Frankel, S.L., and Worden, A.Z, (1996). Dynamics of picophytoplankton, ultraphytoplankton and bacteria in the central equatorial Pacific. Deep-Sea Research II, 43, 907–931.

Brewin, R.J.W., Sathyendranath S., Hirata T., Lavender S.J., Barciela R.M., & Hardman-Mountford N.J., (2010). A three-component model of phytoplankton size class for the Atlantic Ocean. *Ecological Modelling*, *221*, 1472–1483.

Brosnahan, M. L., Velo-Suarez L., Ralston D.K., Fox S.E., Sehein T.R., Shalapyonok A., Sosik H. M., Olson R. J., & Anderson D. M., (2015). Rapid growth and concerted sexual transitions by a bloom of the harmful dinoflagellate *Alexandrium fundyense (*Dinophyceae). Limnology and Oceanography, 60, 2059–2078.

Bustillos-Guzmán, J., Claustre H. & Marty J.C., (1995). Specific phytoplankton signatures and their relationship to hydrographic conditions in the coastal northwestern Mediterranean Sea. Mar. Ecol. Prog. Ser. 124, 247–258.

Campbell, L., Olson, R.J., Sosik, H.M., Araham, A., Henrichs, D.W., Hyatt, C.J., et al., (2010). First harmful Dinophysis (Dinophyceae, Dinophysiales) bloom in the U.S is revealed by automated imaging flow cytometry. J. Phycol. 46, 66–75.

Casotti, R., Landolfi, A. Brunet C., D'Ortenzio F., Mangoni O. & Ribera D'Alcala M., (2003). Composition and dynamics of the phytoplankton of the Ionian Sea (eastern Mediterranean), *J. Geophys. Res.*, *108* (9), 1–19.

Cermeno, P., Maranon E., Perez V., Serret P., Fernandez E., and Castro C. G., (2006). Phytoplankton size structure and primary production in a highly dynamic coastal ecosystem (Ria de Vigo,

NW-Spain): Seasonal and short-time scale variability. Estuarine, Coastal and Shelf Science, 67, 251–266.

Chavez, F.P., Messié, M., Pennington, J.T., (2011). Marine primary production in relation to climate variability and change. Annual Review of Marine Science, 3, 227–260. doi: 10.1146/annurev.marine.010908.163917

Chouvelon, T., Strady, E., Harmelin-Vivien, M., Radakovitch, O., Brach-Papa, C., Crochet, S., Knoery, J., Rozuel, E., Thomas, B., Tronczynski, J., Chiffoleau, J.F., (2019). Patterns of trace metal bioaccumulation and trophic transfer in a phytoplankton-zooplankton-small pelagic fish marine food web, Marine Pollution Bulletin, 146, 1013–1030. doi: 10.1016/j.marpolbul.2019.07.047.

Claustre, H., Kerhervé, P., Marty, J. C., Prieur, L., Videau, C., & Hecq, J.-H., (1994). Phytoplankton dynamics associated with a geostrophic front: ecological and biogeochemical implications, J. Mar. Res., 52, 711–742.

Colella S., D'Ortenzio F., Marullo S., Santoleri R., Ragni,M. & Ribera M. d'Alcala, (2004). Primary production variability in the Mediterranean Sea from SeaWiFS data. Proc. SPIE 5233. https://doi.org/10.1117/12.516791.

Denis, M., Thyssen M., Martin V., Manca B.,.and Vidussi F., (2010). Ultraphytoplankton basin-scale distribution in the eastern Mediterranean Sea in winter: link to hydrodynamism and nutrients. *Biogeosciences*, *7*, 2227–2244.

Dubelaar GB, Gerritzen PL. CytoBuoy: a step forward towards using flow cytometry in operational oceanography. Scimar [Internet] (2000 Jun.30). [cited 2022Jul.14];64(2):255-6. Available from: https://scientiamarina.revistas.csic.es/index.php/scientiamarina/article/view/759

Dugenne, M, (2017). Dynamique du phytoplancton en mer Méditerranée: Approches par mesures à haute fréquence, modélisation, et statistiques bayésiennes, PhD Thesis, Aix Marseille Université, available at: http://www.theses.fr/s137171(last accessed 7 March 2018).

Dugenne M., Thyssen M., Garcia N., Mayot N., Bernard G., and Grégori G.J., (2015). Monitoring of a potential harmful algal species in the Berre lagoon by automated *in situ* flow cytometry, *HJ Ceccaldi et al. (eds), Marine Productivity: Perturbations and Resilience of Socio-ecosystems, Springer 2015*, 117–126.

DuRand M.D., Olson R.J., & Chisholm S.W. (2001). Phytoplankton population dynamics at the Bermuda Atlantic Time-series station in the Sargasso Sea. Deep-Sea Res. II, 48, 1983–2003.

Estrada, M. (1996). Primary production in the northwestern Mediterranean. Sci. Mar., 60(2), 55–64.

Falkowski, P.G., Barber, R.T., Smetacek, V.V., (1998). Biogeochemical controls and feedbacks on ocean primary production. Science, 281, 200–207. doi: 10.1126/science.281.5374.200

Farrant, G.K., Doré, H., Cornejo-Castillo, F.M., Partensky, F., Ratin, M., Ostrowski, M., Pitt, F.D., Wincker, P., Scanlan, D.J., Iudicone, D., Acinas, S.G., & Garczarek, L., (2016). Delineating ecologically significant taxonomic units from global patterns of marine picocyanobacteria, Proc Natl Acad Sci U S A, 113, 3365–3374, https://doi.org/10.1073/pnas.1524865113.

Ferrier-Pages, C. & Rassoulzadegan, F., (1994). Seasonal impact of the microzooplankton on pico- and nanoplankton growth rates in the northwest Mediterranean Sea. Mar. Ecol.-Prog. Ser., 108, 283–294.

Field, C.B., (1998). Primary production of the biosphere: integrating terrestrial and oceanic components, Science, 281, 237–240, https://doi.org/10.1126/science.281.5374.237.

Foladori, P., Quaranta, A. and Ziglio, G. (2008). Use of silica microspheres having refractive index similar to bacteria for conversion of flow cytometric forward light scatter into biovolume. *Water Res.*, *42*, 3757–3766.

Goldman, J.C., McCarthy, J.J. & Peavey, D.G., (1979). Growth rate influence on the chemical composition of phytoplankton in oceanic waters. *Nature*, *279*, 210–215.

Guieu, C., Aumont, O., Paytan, A., Bopp, L., Law, C.S., Mahowald,N., Achterberg, E.P., Marañón, E., Salihoglu, B., Crise, A., Wagener, T., Herut, B., Desboeufs, K., Kanakidou, M., Olgun,

N.,Peters, F., Pulido-Villena, E., Tovar-Sanchez, A., & Völker, C., (2014). The significance of the episodic nature of atmospheric deposition to Low Nutrient Low Chlorophyll regions, Global Biogeochem Cy, 28(11), 1179–1198.

Gutierrez-Rodriguez, A., Latasa M., Estrada M., Vidal M., & Marrase C., 2010. Carbon fluxes through major phytoplankton groups during the spring bloom and post-bloom in the Northwestern Mediterranean Sea. *Deep-Sea Research I, 57,* 486–509.

Hamdi, I., Denis, M., Bellaaj-Zouari, A., Khemakhem, H., Hassen, M. B., Hamza, A., et al., (2015). The characterisation and summer distribution of ultraphytoplankton in the Gulf of Gabès (Eastern Mediterranean Sea, Tunisia) by using flow cytometry. Cont. Shelf Res. 93, 27–38. doi: 10.1016/j.csr.2014.10. 002

Holmes, R.B., Aminot, A., Kérouel, R., Hooker, B.A., Peterson, B.J., 1999. A simple and precise method for measuring ammonium in marine and freshwater ecosystems. Can. J. Fish. Aquat. Sci. 56, 1801–1808.

Hirata, T., Hardman-Mountford N. J., Brewin R. J. W., Alken J., Barlow R., Suzuki K., Isada T., Howell E., Hashioka T., Noguchi-Aita M., and Yamanaka Y., 2011. Synoptic relationships between surface chlorophyll-a and diagnostic pigments specific to phytoplankton functional types. *Biogeosciences*, *8*, 311–327.

Hunter-Cevera, K. R., Neubert, M. G., Solow, A. R., Olson, R. J., Shalapyonok, A., & Sosik, H. M., 2014. Diel size distributions reveal seasonal growth dynamics of a coastal phytoplankter. Proc Natl Acad Sci U S A, 111, 9852–9857, https://doi.org/10.1073/pnas.1321421111.

Jaber, I.B., Abdennadher, J., Boukthir, M., 2014. Pathways of the modified Atlantic water across the Strait of Sicily. Geophys. J. 36 (4), 75–84.

Khammeri, Y., Bellaaj-Zouari, A., Hamza, A., Medhioub, W., Sahli, E., Akrout, F., et al., 2020. Ultraphytoplankton community composition in Southwestern and Eastern Mediterranean

Basin: relationships to water mass properties and nutrients. J. Sea Res. 158:101875. doi: 10.1016/j.seares.2020.101875

Khammeri, Y., Hamza, I.S., Bellaej-Zouari, A., Hamza, A., Sahli, E., Akrout, F., Messaoudi, S., Belhassen, M., 2018. Atmospheric bulk deposition of dissolved nitrogen, phosphorus and silicate in the Gulf of Gabès (South Ionian Basin); implications for marine heterotrophic prokaryotes and ultraphytoplankton. Con. Shelf Res. 159, 1–11. https://doi.org/10.1016/j.csr.2018.03.003.

Latasa, M., Estrada, M. and Delgado, M., 1992. Plankton pigment relationships in the Northwestern Mediterranean during stratification *Mar. Ecol. Progr. Ser.*, *88*, 61-73.

Marina L., 2003. Mesoscale variability of phytoplankton and of new production: Impact of the large scale nutrient distribution. Journal of Geophysical Research, 108 (C11), pp.3358. ff10.1029/2002JC001577ff. ffhal-00153678

Mackey, D.J., Blanchot, J., Higgins, H.W., Neveux, J., 2002. Phytoplankton abundances and community structure in the equatorial Pacific. Deep Sea Res. 49 (13–14), 2561–2582. https://doi.org/10.1016/S0967-0645(02)00048-6.

Magazzu, G. and F. Decembrini, 1995. Primary production, biomass and abundance of phototrophic picoplankton in the Mediterranean Sea: a review. *Aquat. microb. Ecol.*, *9*, 97–104.

Markaki, Z., Loye-Pilot, M.D., Violaki, K., Benyahya, L., Mihalopoulos, N., 2010. Variability of atmospheric deposition of dissolved nitrogen and phosphorus in the Mediterranean and possible link to the anomalous seawater N/P ratio. Mar. Chem. 120 (1–4), 187–194. https://doi.org/10.1016/j.marchem.2008.10.005

Marrec, P., Grégori, G., Doglioli, A. M., Dugenne, M., Della Penna, A., Bhairy, N., Cariou, T., Hélias Nunige, S., Lahbib, S., Rougier, G., Wagener, T., Thyssen, M., 2018. Coupling physics and biogeochemistry thanks to high-resolution observations of the phytoplankton community

structure in the northwestern Mediterranean Sea. Biogeosciences, 15, 1579–1606, https://doi.org/10.5194/bg-15-1579-2018.

Millot C., 1991. Mesoscale and seasonal variability of the circulation in the western Mediterranean. Dynamics of Atmospheres and Oceans. 15, 170-214.

Millot, C. and Taupier-Letage, I., 2005. Circulation in the Mediterranean Sea, The Handbook of Environ. Chem., Springer Berlin, Heidelberg, 323–334.

Morel. A, Ahn, Y, Partensky, F., Vaulot, D., Claustre, H., 1993. Prochlorococcus and Synechococcus: a comparative study of their optical properties in relation to their size and pigmentation. J. Mar. Res, 51: 617-649

Nizzetto, L., Gioia, R., Li, J., Borgå, K., Pomati, F., Bettinetti, R., Dachs, J., Jones, K.C., 2012. Biological pump control of the fate and distribution of hydrophobic organic pollutants in water and plankton. Environ. Sci. Technol. 46 (6), 3204–3211.

Percopo, I., Siano, R., Cerino, F., Sarno, D., and Zingone, A, 2011. Phytoplankton diversity during the spring bloom in the northwestern Mediterranean Sea. Bot. Mar., 54, 243–267, https://doi.org/10.1515/bot.2011.033.

Pittera, J., Humily, F., Thorel, M., Grulois, D., Garczarek, L., & Six, C., 2014. Connecting thermal physiology and latitudinal niche partitioning in marine Synechococcus. ISME J., 8, 1221–1236, https://doi.org/10.1038/ismej.2013.228.

Pulido-Villena E., Baudoux A.-C., Obernosterer I., Landa M.,Caparros J., Catala P., Georges C., Harmand J., Guieu,C, 2014. Microbial food web dynamics in response to a Saharan dust event: results from a mesocosm study in the oligotrophic Mediterranean Sea. Biogeosciences Discuss., 11, 337–371, doi:10.5194/bgd-11-337-2014.

Quéméneur M, Bel Hassen M, Armougom F, Khammeri Y, Lajnef R, Bellaaj-Zouari A., 2020. Prokaryotic Diversity and Distribution Along Physical and Nutrient Gradients in the Tunisian

Coastal Waters (South Mediterranean Sea). Front Microbiol. Dec 1; 11:593540. doi: 10.3389/fmicb.2020.593540. PMID: 33335519; PMCID: PMC7735998.

Redfield, A.C., Ketchum, B.H., Richards, F.A., 1963. The influence of organisms in the composition of seawater. In Hill, M.N. (Ed.), The sea, Vol II. Wiley,New York, pp. 26–77.

Ribalet, F., Swalwell, J., Clayton, S., Jiménez, V., Sudek, S., Lin, Y., Johnson, Z. I., Worden, A. Z., and Armbrust, E. V., 2015. Light-driven synchrony of Prochlorococcus growth and mortality in the subtropical Pacific gyre Proc Natl Acad Sci U S A, 112, 8008–8012, https://doi.org/10.1073/pnas.1424279112.

Raimbault, P, Rodier, M., Taupier-Letage, I., 1988. Size fraction of phytoplankton in the Ligurian Sea and the Algerian Basin (Mediterranean Sea): size distribution versus total concentration. Mar. Microb. Food Webs.

Sakka, H.A., Niquil, N., Legendre, L., 2014. Planktonic food webs revisited: Reanalysis of results from the linear inverse approach. Prog. Ocea. 120, 216–229. https://doi.org/ 10.1016/j.pocean.2013.09.003.

Shalapyonok, A., Olson, R. J., and Shalapyonok, L. S.,2001. Arabian Sea phytoplankton during Southwest and Northeast Monsoons 1995: composition, size structure and biomass from individual cell properties measured by flow cytometry. Deep-Sea Res. Pt. II, 48, 1231–1261.

Siegenthaler, U., Sarmiento J. L., 1993. Atmospheric carbon dioxide and the ocean. *Nature*, *365*, 119–125.

Sobek, A., Gustafsson, O., 2004. Latitudinal fractionation of polychlorinated biphenyls in surface seawater along a 62°N–89°N transect from the southern Norwegian Sea to the North Pole area. Environ. Sci. Technol. 38, 2746–2751.

Sosik, H. M., Olson, R. J., Neubert, M. G., Shalapyonok, A., and Solow, A. R.,2003. Growth rates of coastal phytoplankton from time-series measurements with a submersible flow cytometer. Limnol. Oceanogr., 48, 1756–1765, https://doi.org/10.4319/lo.2003.48.5.1756.

Steele, J.H., 1962. Environmental control of photosynthesis in the sea. Limnol Oceanogr, 7, 137–150.

Taylor, B.W., Keep, C.F., Hall, R.O., Koch, B.J., Tronstad, L.M., Flecker, A.S., and Ulseth, A.J., 2007. Improving the fluorometric ammonium method: matrix effects, background fluorescence, and standard additions. Journal of the North American Benthological Society 26, 167-177.

Tedetti, M., Tronczynski, J., 2019. HIPPOCAMPE cruise, RV Antea, https://doi.org/10.17600/18000900

Tedetti, M., et al. Contamination of planktonic trophic webs in the Mediterranean Sea: Introduction to the MERITE-HIPPOCAMPE oceanographic cruise (spring 2019). In preparation, this issue.

Vaulot, D. & Marie, D., 1999. Diel variability of photosynthetic picoplankton in the equatorial Pacific. J. Geophys. Res.-Oceans, 104, 3297–3310, https://doi.org/10.1029/98JC01333.

Verity, P.G., Robertson C.Y., Tronzo C.R., Andrews M.G., Nelson J.R., Sieracki M.E., 1992. Relationships between cell volume and the carbon and nitrogen content of marine photosynthetic nanoplankton Limnol.Oceanogr, 37 (7), 1434–1446.

Vidussi, F., Marty J-C., and Chiavérini J., 2000. Phytoplankton pigment variations during the transition from spring bloom to oligotrophy in the northwestern Mediterranean Sea. Deep-Sea Research I, 47, 423–445.

Vidussi, F., Claustre, H., Manca, B. B., Luchetta, A., and Marty, J.-C., 2001. Phytoplankton pigment distribution in relation to upper thermocline circulation in the eastern Mediterranean Sea during winter. *J. Geophys. Res.*, 106(C9), 19939– 19956, doi:10.1029/1999JC000308.

Wallberg, P., Bergqvist, P.A., Anderson, A., 1997. Potential importance of protozoan grazing on the accumulation of polychlorinated biphenyls in the pelagic food web. Hydrobiologia 357, 53–62.

Zhou, Q., Chen W., Zhang H., Peng L., Liu L., Han Z., Wan N., Li L., Song L., 2012. A flow cytometer-based protocol for quantitative analysis of bloom forming cyanobacteria (*Microcystis*) in lake sediments. *J. Env. Sciences, 24* (9), 1709–1716.

Table 1. Main characteristics of the ten stations sampled along a North-South Mediterranean transect during the MERITE-HIPPOCAMPE cruise (13 April-14 May 2019). (a) The SOLEMIO station (Site d'Observation Littoral pour l'Environnement du MIO) is part of the French national network of coastal observation SOMLIT (Service d'Observation en Milieu LITtoral – http://somlit.epoc.u-bordeaux1.fr/fr/). (b) The JULIO station (JUdicious Location for Intrusions Observations) is dedicated to the study of the intrusions of Liguria current. (c) The PEACETIME cruise (ProcEss studies at the Air-sEa Interface after dust deposition in the MEditerranean sea) took place in May-June 2017 (http://peacetime-project.org/) (d) Consensus ecoregions of the Mediterranean Sea as defined by Ayata et al. (2018).

Station	Latitude (N)	Longitude (E)	Location	Characteristics	Depth (m)	Period
St2	42° 56.020'	5° 58.041'	Toulon – offshore (Maures Escarpement)	Limit of the continental shelf; Boundary of the Ligurian ecoregion[d]	1770	14-16/04
St4	43° 14.500'	5° 17.500'	Bay of Marseille (SOLEMIO[a] station)	Urbanized bay	58	16-18/04
St3	43° 08.150'	5° 15.280'	Marseille – offshore (JULIO[b] station)	Southeast entrance to the Gulf of Lion; Liguria current intrusions	95	18-20/04
St10	40° 18.632'	7° 14.753'	Offshore (PEACETIME[c] 2 station)	Near the North thermal front of the Balearic Islands	2791	22-24/04
St11	39° 07.998'	7° 41.010'	Offshore (PEACETIME[c] 3 station)	Algerian ecoregion[d]; Gyres, intermediate primary production	1378	25-26/04
St15	36° 12.883'	11° 07.641'	Gulf of Hammamet	Phytoplankton area and high density of small pelagic fishes	100	29-30/04
St17	34° 30.113'	11° 43.573'	Boundary Gulf of Gabes	Gabès ecoregion[d] boundary; High density of small pelagic fishes	48	01-02/05
St19	33° 51.659'	11° 18.509'	Gulf of Gabes – South	Gabès ecoregion[d]; High density of small pelagic fishes and phytoplankton area	50	02-05/05
St9	41° 53.508'	6° 19.998'	Offshore (PEACETIME[c] 1 station)	Ligurian ecoregion[d] boundary	2575	08-09/05
St1	43° 03.819'	5° 59.080'	Bay of Toulon	Urbanized bay	91	10-11/05
Zarzis	33° 37.952'	11° 17.73'	Zarzis	Saharan dust deposit	30	03-04/05

Table 2. Mean and SD of FWS, estimated size and biovolume of the Synechoccocus, picoeukaryotes, nanoeukaryotes and Cryptophytes-like (1) Verity et al. (1992), (2) Campbell et al. (1994) and Shalapyonok et al. (2001), (3) Marrec et al. (2018)

Parameters	Synechoccocus	Picoeukaryotes	Nanoeukaryotes	Cryptophytes-like
FWS (a.u. cell^{-1})	292.4 ± 110	6078 ± 1480	34200 ± 4395	91200 ± 47049
Estimated size (µm)	1.05 ± 0.09	2.46 ± 0.19	4.15 ± 0.16	5.59 ± 0.77
Biovolume (µm^3 cell^{-1})	0.60 ± 0.17	7.76 ± 1.72	37.43 ± 4.36	91.47 ± 42.12
Conversion coefficients (a,b)	(0.39,0.86)[1]	(0.32,0.8666)[1]	(0.27,0.8666)[1]	(0.25,0.8666)[1]
Calculated Qc,cal (fg C cell^{-1})	253	1871	6258	12273
Literature Qc (fg C cell^{-1})	100[(3)]-250[(2)]	2108[(2)]	9000[(3)]	-

Table 3. Community contribution by zone in terms of abundance (cells cm^{-3}), biomass (µg C m^{-3}) and total FLR (a.u. cm^3) (Syn= *Synechococcus*, Pico= picoeukaryotes, Nano=nanoeukaryotes, Cry=Cryptophytes-like)

Zone	Abundance (%)				Biomass (%)				Red fluorescence (%)			
	Syn	***Pico***	***Nano***	***Cry***	***Syn***	***Pico***	***Nano***	***Cry***	***Syn***	***Pico***	***Nano***	***Cry***
Z1	79.2 *±15.5*	7.5 *±10.1*	11.6 *±6.4*	0.7 *±0.3*	19.3 *±17.6*	11.1 *±5.5*	62.1 *±13.5*	7.0 *±2.0*	18.9 *±15.0*	8.3 *±3.2*	60.9 *±9.7*	8.4 *±6.4*
Z2	80.6 *±14.2*	5.3 *±4.8*	12.9 *±9.4*	1.7 *±0.4*	17.1 *±10.3*	6.4 *±2.9*	63.9 *±10.5*	12.6 *±3.4*	9.9 *±7.8*	3.8 *±2.4*	73.2 *±8.1*	12.9 *±3.5*
Z3	59.1 *±18.8*	18.5 *±6.7*	19.7 *±13.1*	0.6 *±0.3*	7.7 *±5.4*	19.2 *±4.3*	68.5 *±8.3*	3.6 *±1.0*	8.9 *±7.8*	13.9 *±2.9*	70.8 *±8.5*	5.1 *±1.9*
Z4	70.1 *±18.4*	11.5 *±6.8*	16.6 *±12.1*	0.2 *±0.1*	11.8 *±8.9*	16.6 *±3.1*	69.2 *±9.9*	2.4 *±1.0*	11.8 *±9.3*	12.7 *±2.3*	71.5 *±8.9*	3.6 *±1.8*
Z5	74.6 *±12.3*	12.3 *±6.2*	12.4 *±6.3*	0.3 *±0.1*	13.7 *±7.9*	16.0 *±2.3*	65.3 *±6.9*	4.0 *±0.8*	12.4 *±8.4*	15.7 *±3.9*	64.8 *±6.4*	6.9 *±2.5*
Z6	80.1 *±11.2*	9.4 *±4.9*	10.5 *±6.8*	0.3 *±0.2*	16.1 *±6.8*	17.7 *±3.7*	61.9 *±7.2*	3.7 *±1.0*	17.0 *±7.7*	13.8 *±3.3*	64.8 *±7.3*	5.2 *±1.8*
Z7	81.0 *±2.1*	8.4 *±1.8*	9.0 *±1.5*	1.3 *±0.3*	22.6 *±3.4*	12.2 *±2.4*	51.5 *±2.5*	13.2 *±2.6*	15.1 *±2.2*	10.1 *±2.0*	63.6 *±2.4*	10.9 *±1.4*

Table 4. NPP production per ultraphytoplankton group (mg C m^{-3} d^{-1}) (min, max and mean under brackets) values calculated using Equation (3) by zone.

Group	***Z1***	***Z2***	***Z3***	***Z4***	***Z5***	***Z6***	***Z7***
Synechoccocus	1.3-12.0 (4.8)	13.9-23.1 (18.5)	0.8-4.8 (2.2)	0.3-4.1 (1.6)	0.4-2.6 (1.2)	0.7-4.2 (5.2)	0.9-9.4 (3.0)
Picoeukaryotes	0.6-5.2 (2.4)	2.6-3.1 (2.8)	1.1-2.4 (1.6)	0.4-3.3 (1.7)	0.4-1.2 (0.8)	0.6-7.9 (1.3)	0.5-2.1 (2.7)
Nanoeukaryotes	0.7-14.6 (5.3)	8.1-14.9 (11.5)	1.9-6.2 (3.4)	0.7-3.3 (1.7)	0.5-0.7 (0.7)	1.6-5.0 (4.0)	0.9-7.1 (2.6)
Cryptophytes-like	1.0-12.5 (3.3)	3.1-4.4 (3.8)	0.7-4.1 (1.7)	0.3-1.8 (0.8)	0.2-0.9 (0.6)	0.3-4.6 (1.2)	0.6-1.7 (1.9)

Figure(s)

Click here to access/download;Figure(s);renamed_a6199.docx

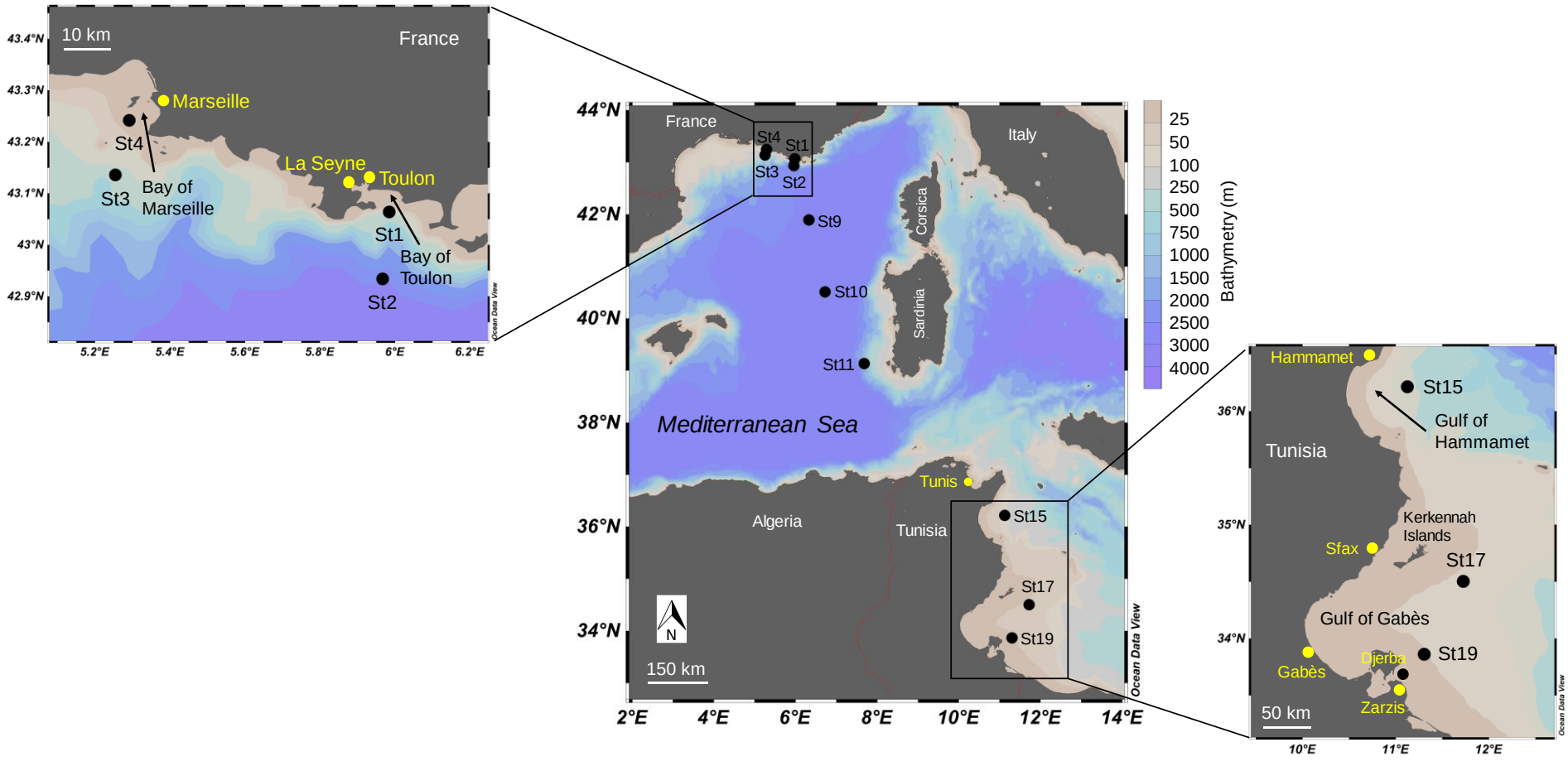

Figure 1 Map of the MERITE-HIPPOCAMPE cruise track in the Mediterranean Sea with the positions of the ten stations sampled.

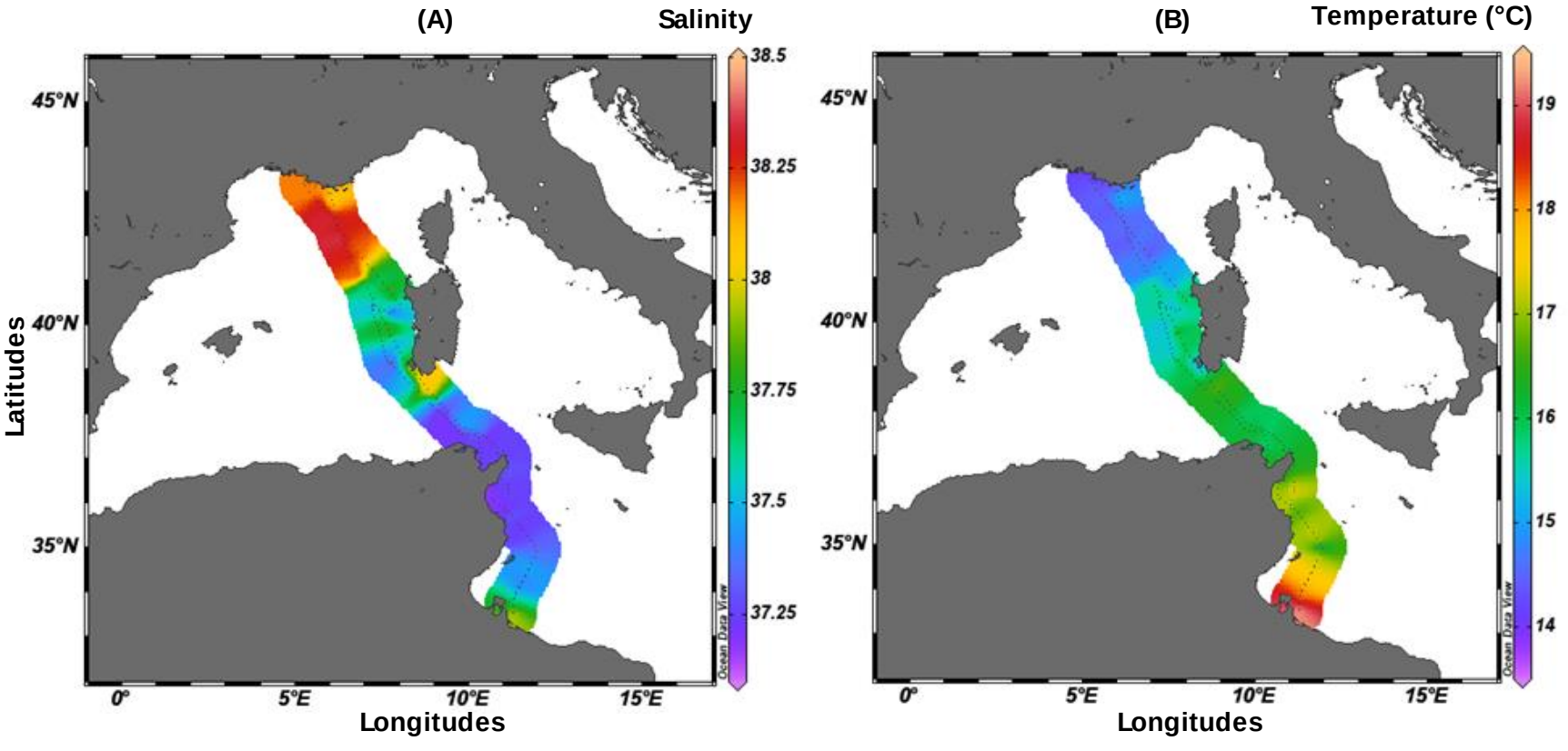

Figure 2 Subsurface temperature (A) and salinity (B) distributions along the Mediterranean transect during the MERITE-HIPPOCAMPE cruise

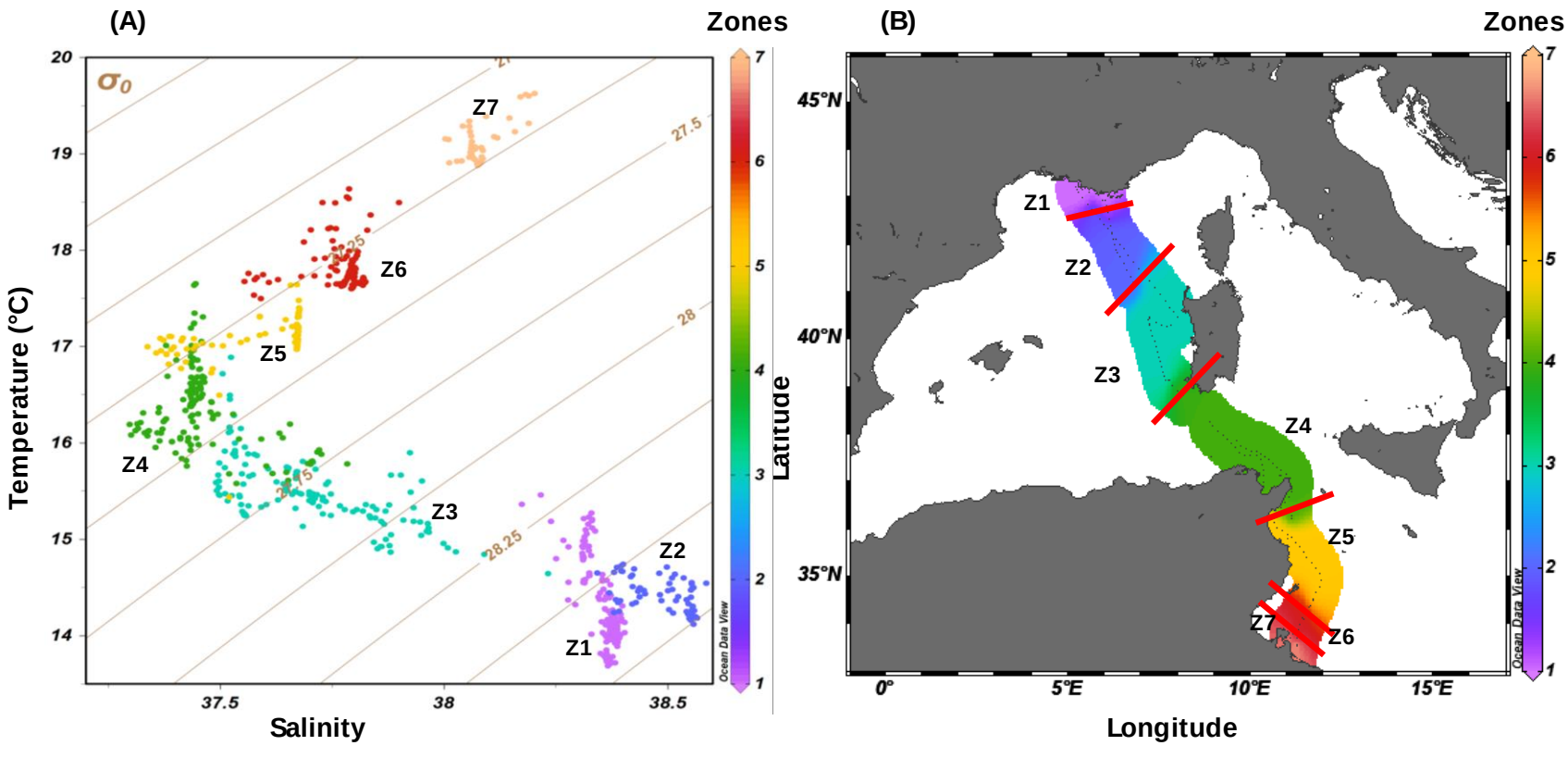

Figure 3 Temperature vs salinity of subsurface waters (A) sampled at 2-m depth. Surface distribution of the 7 zones along the round trip transect (B).

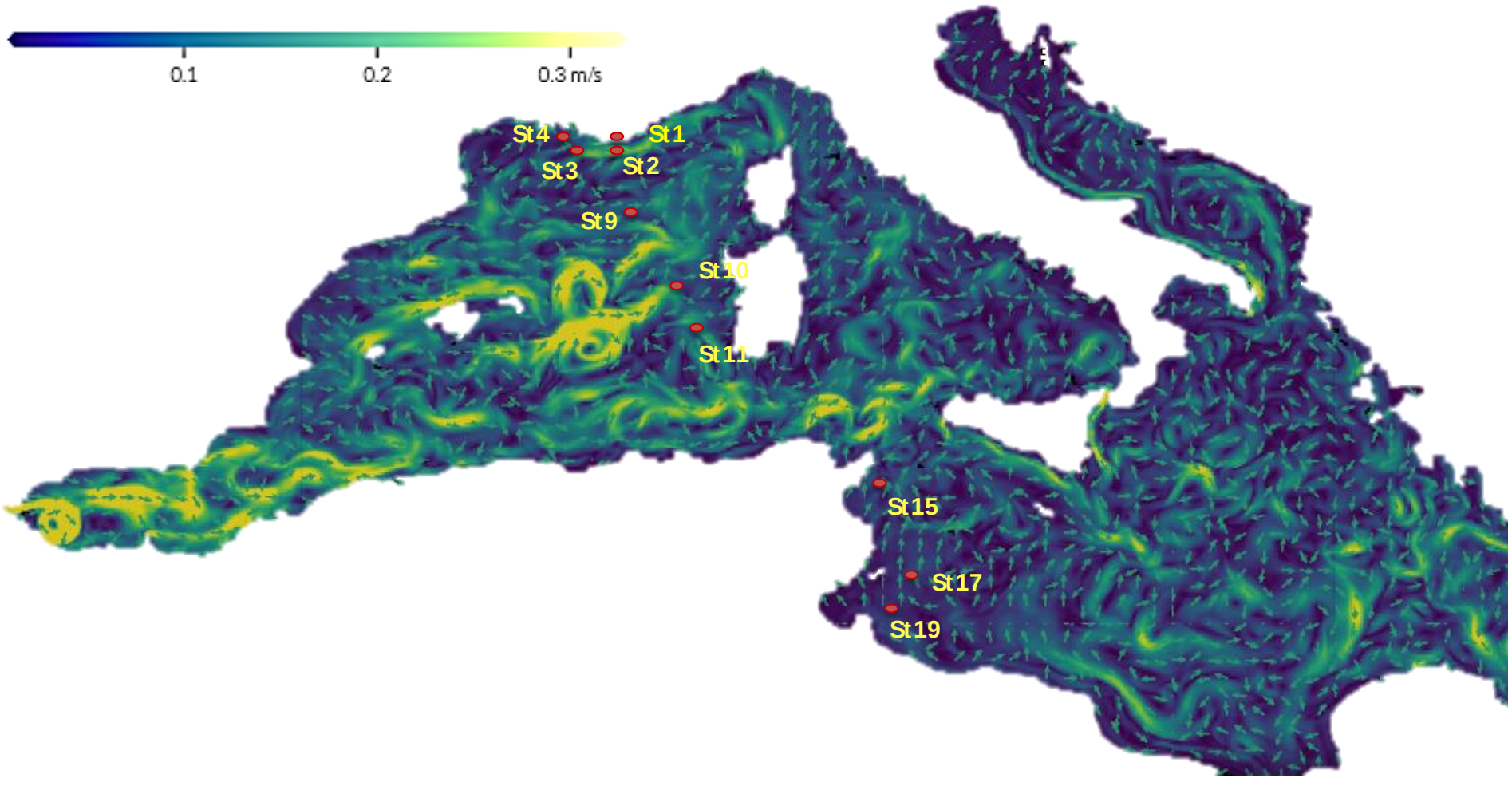

Figure 4 Surface water velocity map of the Mediterranean Sea on May 8th, 2019 (from MyOcean Pro COPERNICUS online interface)

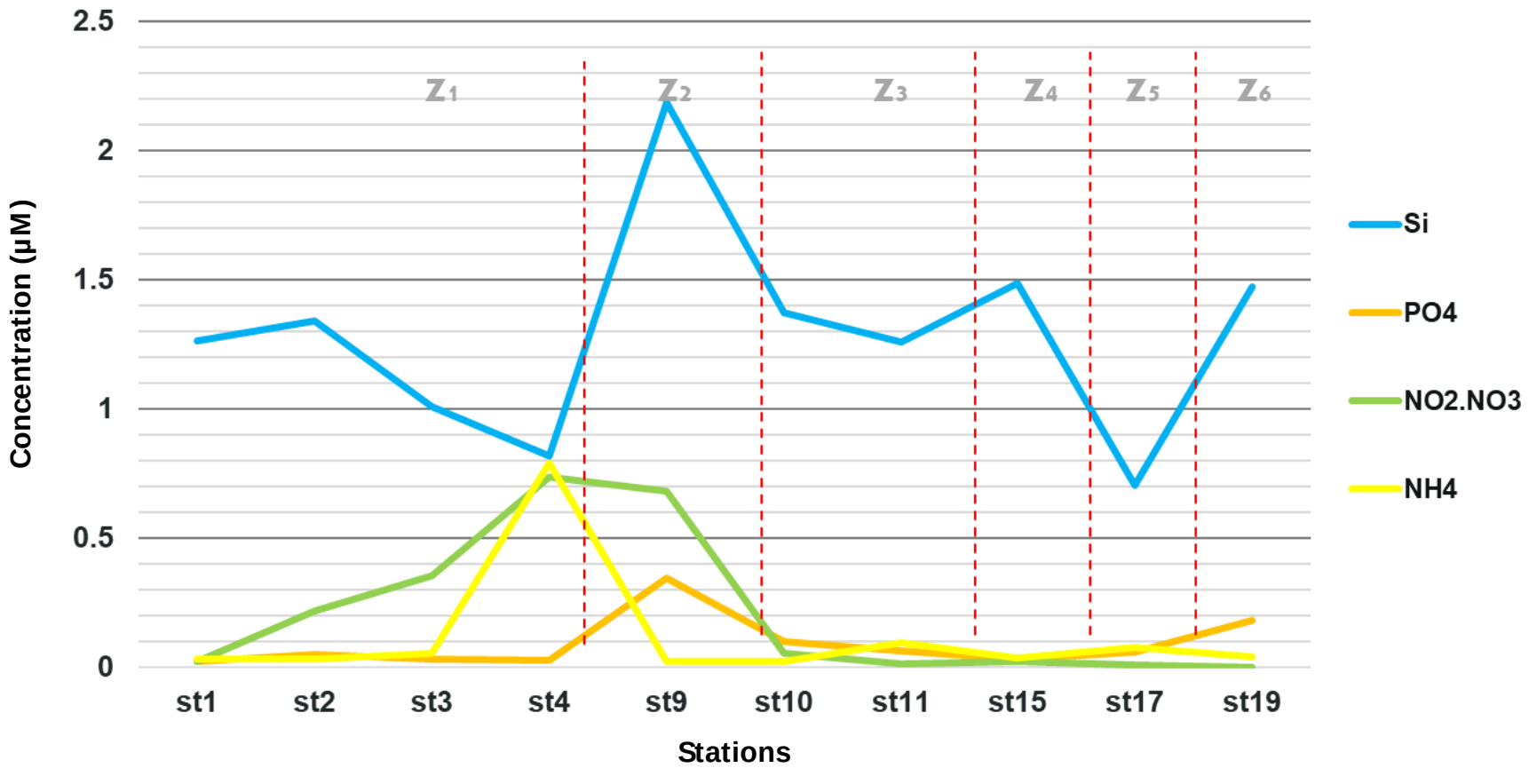

Figure 5 Concentrations (µM) of $Si(OH)_4$ (blue line), PO_4^{3-} (orange line), $NO_3^- + NO_2^-$ (green line) and NH_4^+ (yellow line) in subsurface waters (5-m depth) at the ten stations. Zone 7, which does not contain any of the ten stations (and thus no nutrient data), is not displayed here.

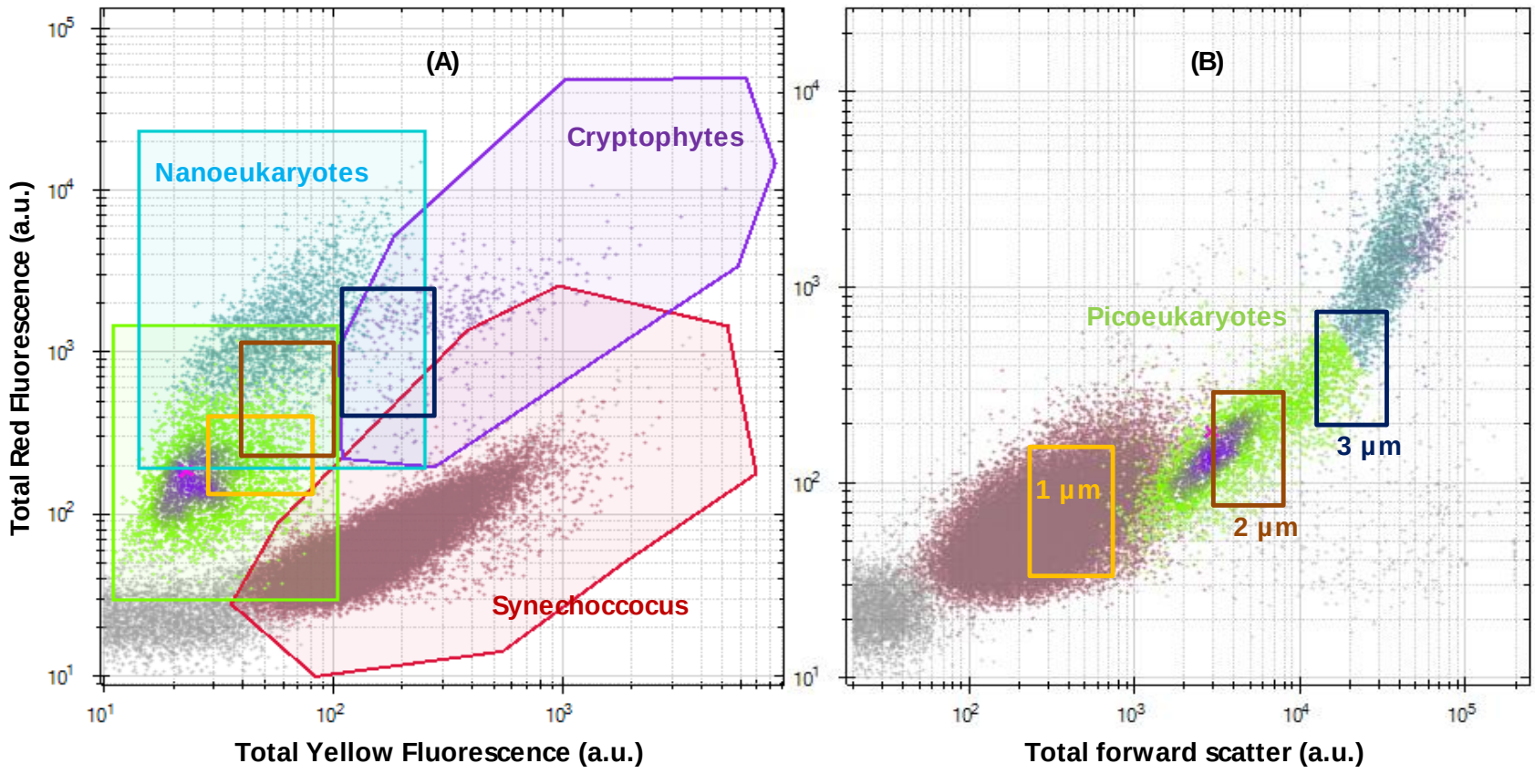

Figure 6. Cytograms representing the Total Red Fluorescence (Total stands for area under the pulse shape curve, a.u.) vs Total Yellow Fluorescence (a.u.) signatures used to classify Synechococcus and Cryptophytes-like (A) and the Total Red fluorescence (a.u.) vs the Total Forward scatter (a.u.) for the classification of picoeukaryotes and nanoeukaryotes (B). Scares represent the areas where silica beads are observed as a memory footprint for size classification.

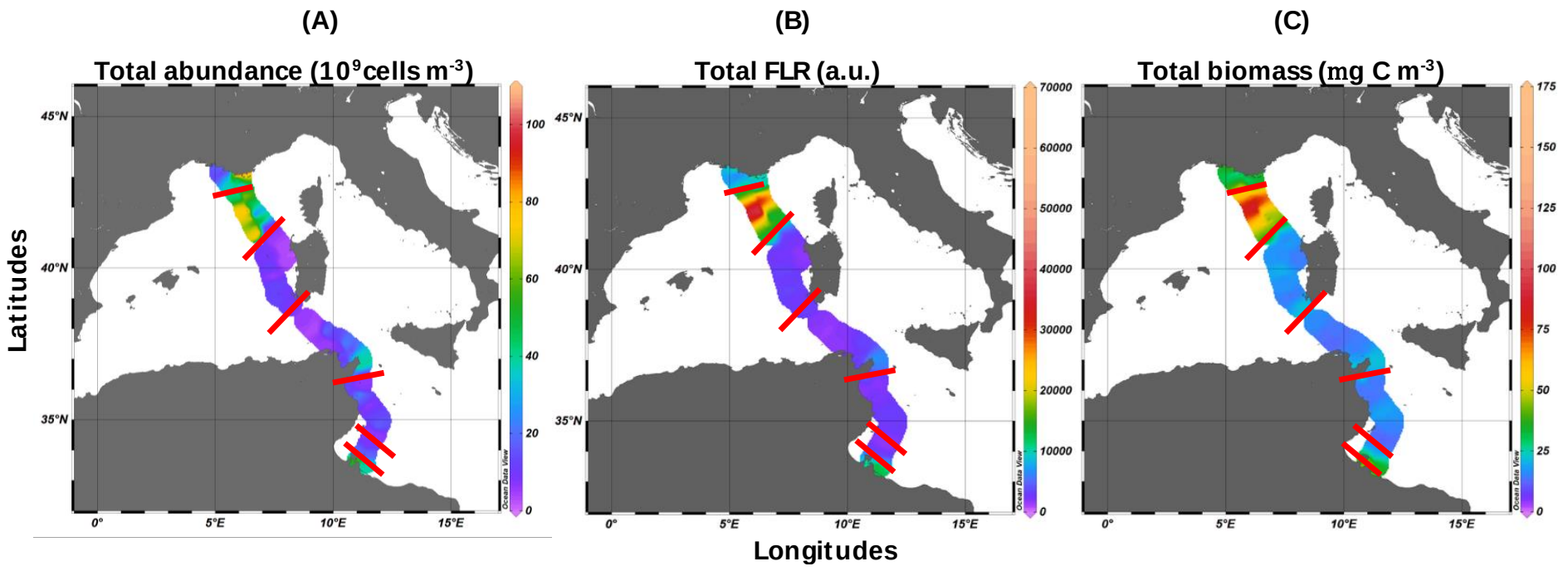

Figure 7. Distribution of total (sum of each ultraphytoplankton group) abundance (10^{-3} cells m^{-3}) (A), FLR per unit of volume (a.u. m^{-3}) (B), and biomass (mg C m^{-3}) (C) in the subsurface waters of the round trip transect.

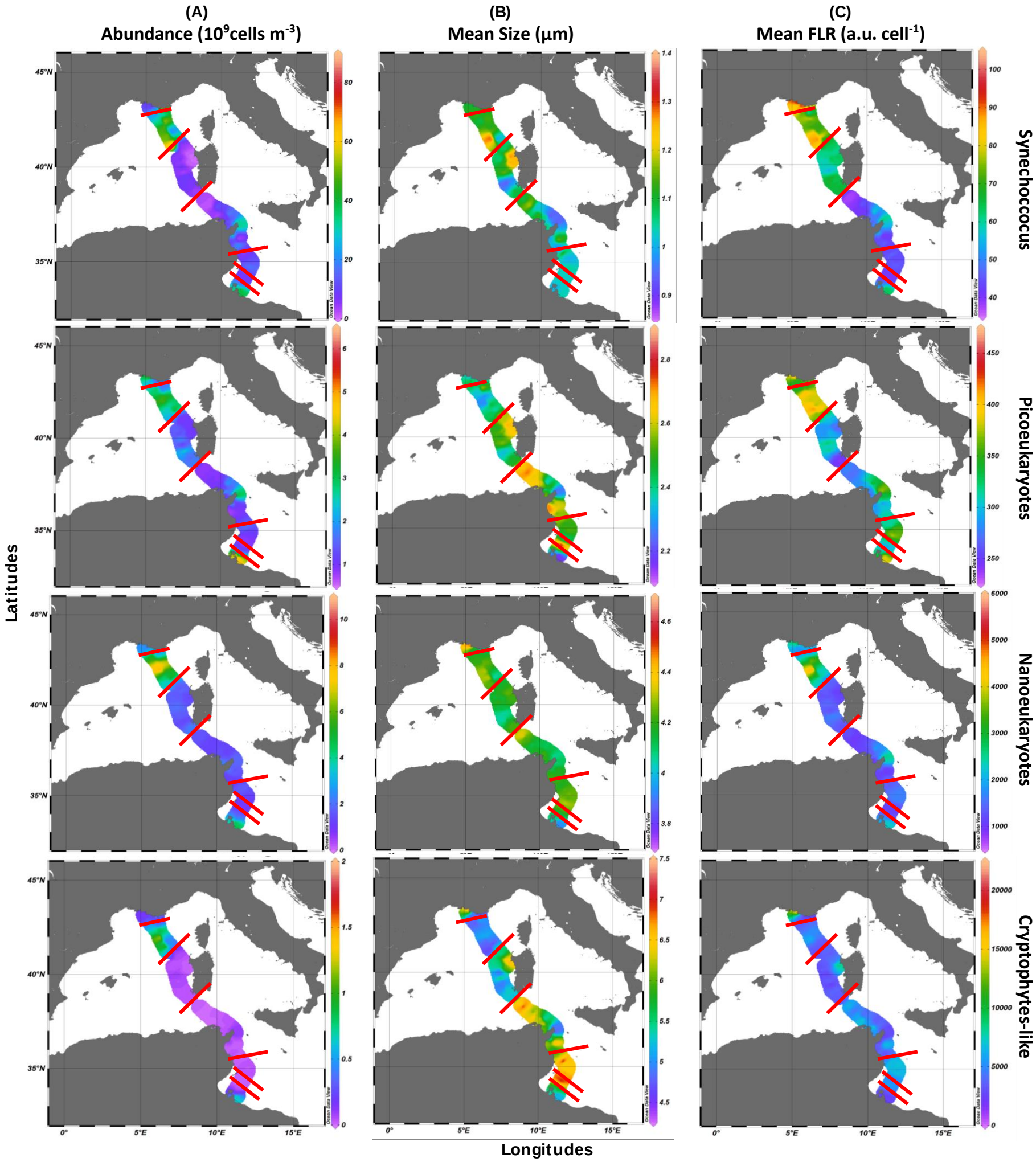

Figure 8 Spatial distribution of the abundances (10^9 cells m^{-3}) (A), mean cell size (µm) (B) and mean FLR (a.u. cell^{-1}) for the four resolved groups. Red lines represents the 7 zones (Z1 to Z7) generated by hierarchical classification.

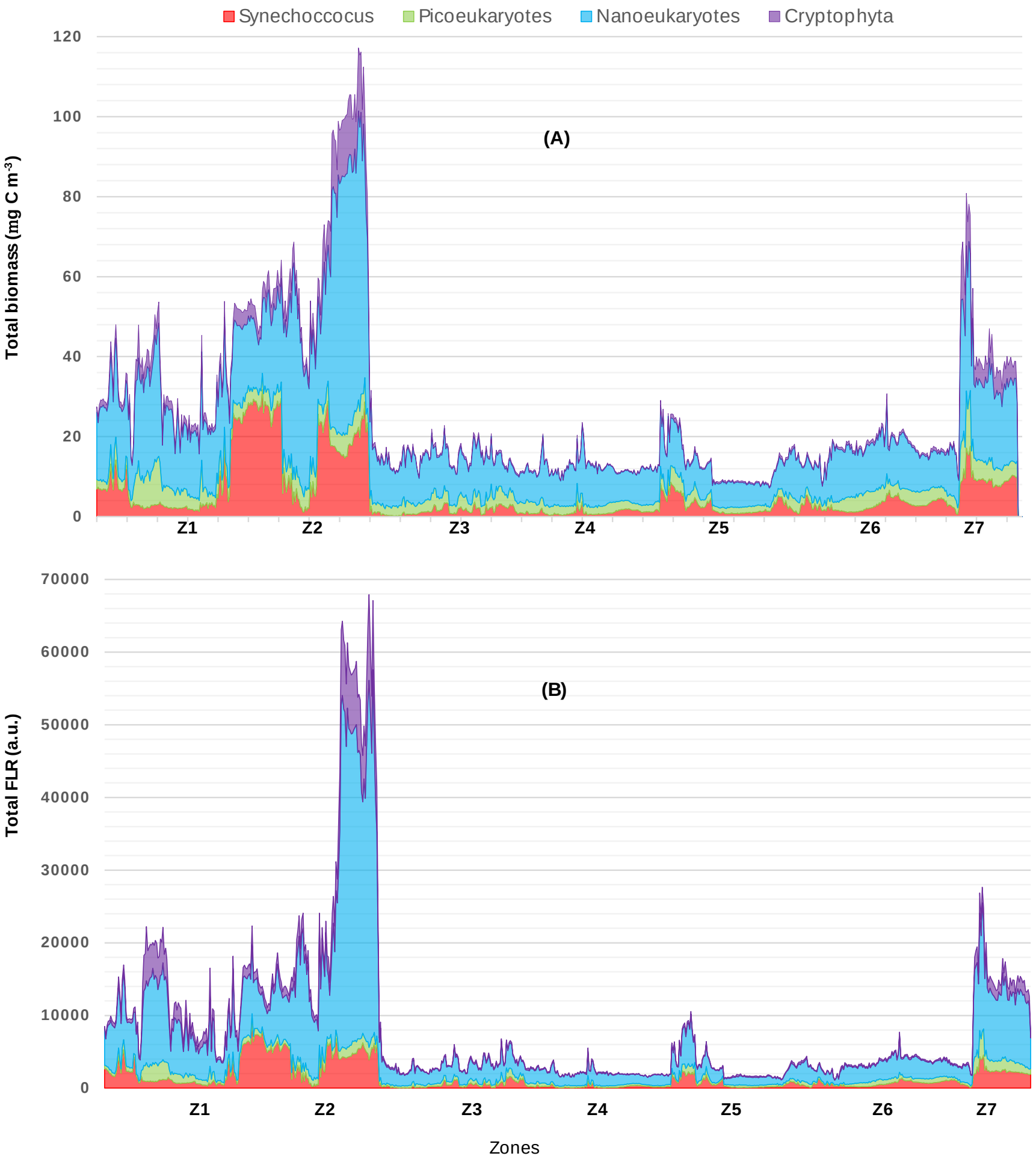

Figure 9 Total biomass contribution of Synechoccocus, picoeukaryotes, nanoeukaryotes and Cryptophytes-like along the 7 zones in terms of biomass (mg C m^{-3}) (A) and FLR_{cell} (B)

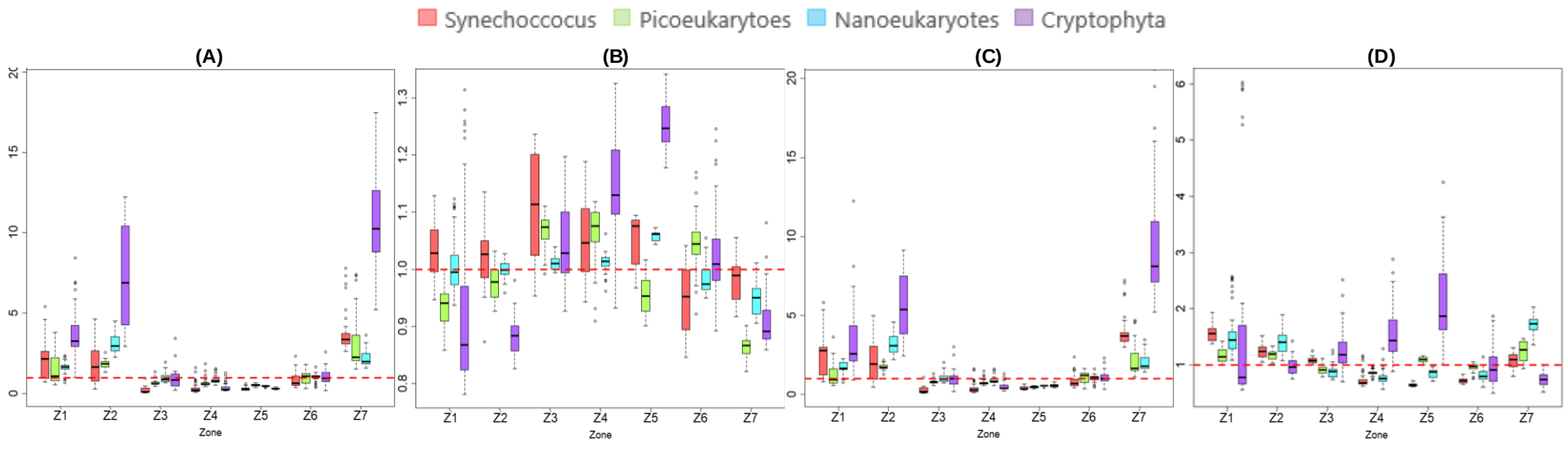

Figure 10 Spatial variability of median-normalized abundance (A), mean size (B), FLR_{cell} (C) and biomass (D) for each ultraphytoplankton group; with red line representing the normalized median =1

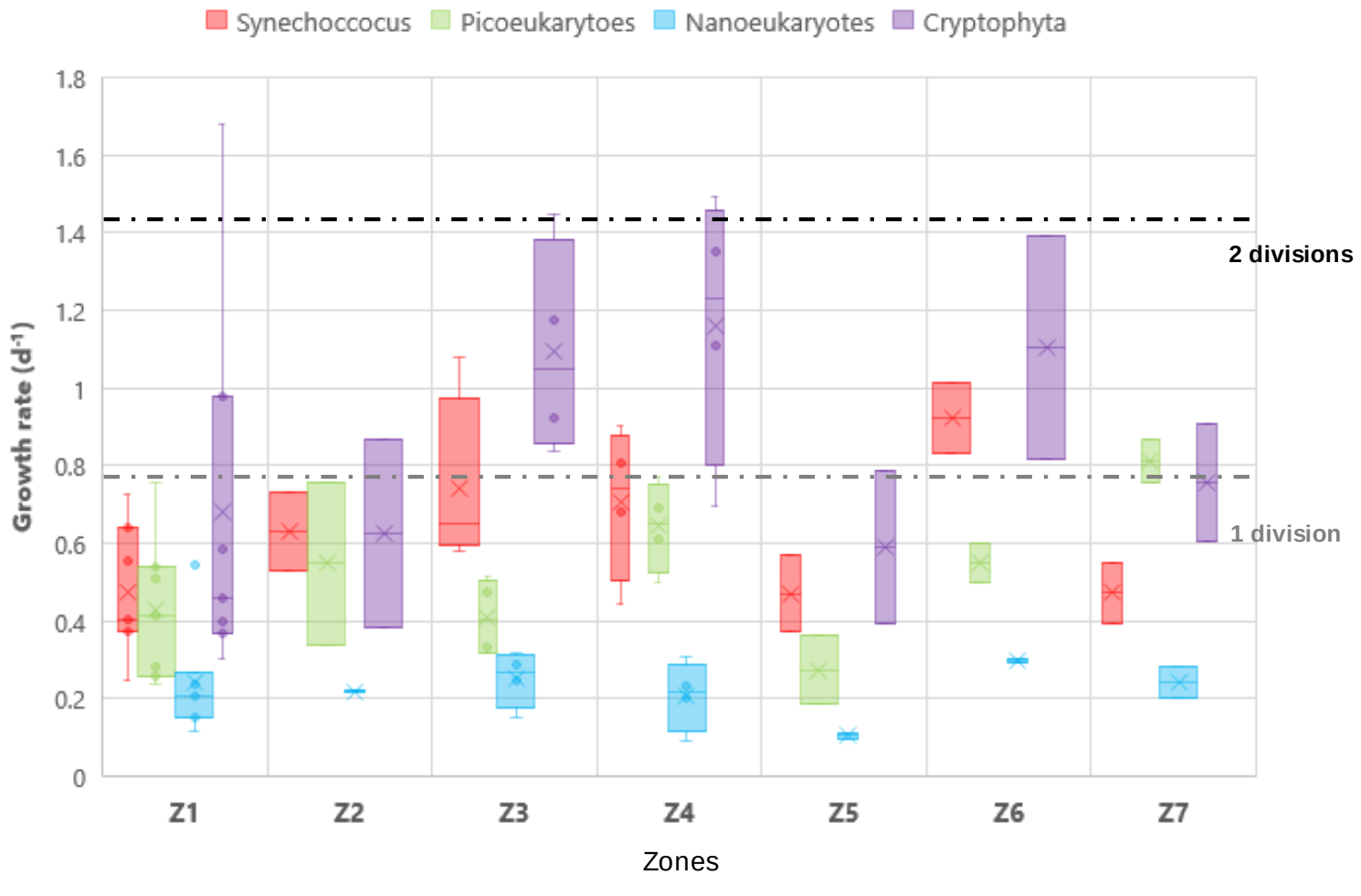

Figure 11 Growth rate variation by zones for the Synechoccocus, picoeukaryotes, nanoeukaryotes and Cryptophytes-like with 0.69 (grey dotted line) and 1.38 (black dotted line) respectively corresponding to 1 and 2 divisions per day